in atherogenesis, by damaging and activating the endothelium, oxidizing low-density lipoprotein (LDL) cholesterol, and promoting proliferation of vascular smooth muscle cells. They also induce various genes such as those of adhesion molecules and chemokines, which play important roles in the initiation and progression of atherosclerotic lesion formation [8,9].

ACE inhibitors (ACE-I) and Ang II type 1 receptor blockers (ARB) are widely used for treatment of hypertension to prevent organ damages. These drugs have been already reported to prevent atherosclerosis in several studies using animal models [10–13]. Losartan reduced atherosclerotic lesion formation without changing blood pressure in cynomologous monkeys [10] and apolipoprotein E-deficient (apoE-KO) mice [11]. Olmesartan was reported to reduce atherosclerosis in association with suppressions of serum macrophage-colony stimulating factor, transforming growth factor-beta 1 and intracellular adhesion molecule-1 in monkeys fed a high cholesterol chow [13].

There has been little information whether ARB can show anti-atherogenic effects by the mechanisms related to suppression of oxidative stress. In the present study, we investigated the effects of telmisartan, an ARB, on atherosclerotic lesion formation in apoE-KO mice. Particularly, we examined whether the effects of telmisartan on atherogenesis were independent of its effect on blood pressure and associated with changes in oxidative stress.

2. Materials and methods

2.1. Materials and animal preparation

Telmisartan was obtained from Boehringer Ingelheim Inc. (Germany). All other commercial drugs used in this study were purchased from Sigma Chemical Co. (MO). ApoE-KO mice on a C57BL/6 genetic background at 4 weeks of age were assigned to control group and two telmisartan-treatment groups given different dosages. Drug treatment consisted of 0.3 and 3 mg/kg body weight per day of telmisartan dissolved in drinking water. Mice were fed a standard chow and supplemented with telmisartan for next 12 weeks and sacrificed at 16 weeks of age. Animals were provided the chow and water ad libitium and maintained on a 12 h light/dark cycle. All animal experiments were conducted according to the guidelines for animal experiments at Kobe University Graduate School of Medicine.

2.2. Plasma analysis

After overnight fasting, blood was collected by the cardiac puncture into heparin-coated tubes under anesthetic condition using pentobarbital sodium (80 mg/kg intraperitoneal injection). Plasma was obtained through centrifugation of the blood for 10 min at 5500 × *g* at 4 °C and stored at −80 °C until each assay. Concentrations of plasma total cholesterol and triglyceride were determined by use of an automated clinical chemistry analyzer. High-density lipoprotein cholesterol levels were quantified by enzymatic reaction using a commercially available kit (Wako, Japan). Glucose levels were determined by glucometer (Sanwa Kagaku, Japan) and insulin levels were determined with a commercially available kit (LINCO Research Inc., MO).

2.3. Hemodynamic analysis

Heart rate and systolic blood pressure of apoE-KO mice were measured at 16 weeks of age using the tail-cuff method without heating. The mouse tail was placed into a device with a rubber cuff and a photoelectric sensor, and heart rate and systolic blood pressure were measured using MK-2000 (Muromachi Kikai, Japan). All measurements were repeated six times for each mouse.

2.4. Atherosclerotic lesion assessment at the aortic sinus

After 12 weeks of telmisartan treatment, both gender mice (16 weeks of age) were anesthetized as above and the aorta was perfused with normal saline containing 10 U/ml heparin. Then the aorta sample was dissected from the middle of the left ventricle to the aortic arch, and fixed with 4% paraformaldehyde for overnight. The sample was cut in the ascending aorta, and the proximal sample containing the aortic sinus was embedded in OCT compounds (Tissue-Tek, CA). Five consecutive sections (10 μm thickness), spanning 550 μm of the aortic sinus, were collected from each mouse and stained with Sudan III and Masson's trichrome. For quantitative analysis of atherosclerosis, the average lesion area of five separate sections from each mouse was obtained with the use of the Image J (National Institutes of Health, MD) according to the method described by Paigen et al. [14].

2.5. Immunohistochemistry

Immunohistochemical staining with MOMA-2 (BMA Biomedicals AG, Switzerland; 1:500 dilution), malondialdehyde (MDA) (Alpha Diagnostic International Inc., TX; 1:100 dilution) and 4-hydroxy-2-nonenal (HNE) (Alpha Diagnostic International Inc., TX; 1:100 dilution) of atherosclerotic lesions at the aortic sinus was performed by the labeled streptaviadin biotin method as previously reported [15]. Quantitative analysis of MOMA-2-immunostaining was evaluated as a ratio of the positive-stained area to total plaque area in the atherosclerotic lesion at the aortic sinus.

2.6. Measurement of superoxide production from aortas

After euthanization of mice, the aorta was cut out from the aortic arch to the bifurcation of iliac arteries and the tissues around the vessel were cleaned. Then the aorta were cut into four pieces (approximately 5 mm length per each pieces) and

these aortic rings were incubated with the Cu–Zn superoxide dismutase inhibitor for 30 min at 37 °C, and vascular superoxide production levels were measured by chemiluminescence (CL) with 10 μM lucigenin (bis-*N*-methylacridinium nitrate). The final volume of lucigenin solution was 1 mL. The light reaction between superoxide and lucigenin was detected with a BLR-201 CL reader (ALOKA, Japan) and photon emission was continuously recorded for 15 min. The CL signal was expressed as the average count per minute (C.P.M.) for 15 min periods and the counts were corrected by vessel dry weights.

2.7. Measurement of NAD(P)H dependent oxidase activity of aorta homogenates

The aorta was cut out from each mouse as described above, and the aortic segments (almost 2 cm length) were placed in a chilled modified 50 mM HEPES/PSS buffer and homogenized on ice with a motor-driven tissue homogenizerfor 1 min in 200 μL homogenate buffer, which contained 0.01 mM EDTA. The homogenates were centrifuged at 1000 × *g* for 10 min. The pellet was discarded and the supernatant was stored on ice until use. Protein concentration of aorta homogenate was measured by the method of Bradford [16]. The assay solution contained 50 mM HEPES/PSS (pH 7.4), 1 mM EDTA, 6.5 mM $MgCl_2$, 83 mM sucrose, and 250 μM lucigenin as the electron acceptor and 100 μM NADH or 100 μM NADPH as the electron donor [17]. After pre-incubation at 37 °C for 20 min, the reaction was started by adding 20 μL of aorta homogenates. All CL data were evaluated after subtracting the CL counts obtained in the absence of homogenates. Each count was corrected by protein levels of aorta homogenate.

In some experiments, we examined the effects of 100 μM diphenylene iodonium (DPI), an inhibitor of all flavoenzymes, and 500 μM apocynin, an inhibitor of NAD(P)H oxidase, on superoxide production after stimulation of homogenates with NAD(P)H. The aorta homogenates were pre-incubated with each agent for 15 min before CL measurement.

2.8. In situ detection of superoxide production in aortas and endothelial cells

To evaluate in situ superoxide production from vessels, unfixed frozen cross sections of aortas were stained with dihydroethidium (DHE; Molecular Probe, OR) according to the previously validated method [18]. In the presence of superoxide, DHE is converted to the fluorescent molecule ethidium, which can then label nuclei by intercalating with DNA. Briefly, the unfixed frozen tissues were cut into 10 μm thick sections, and incubated with 10 μM DHE at 37 °C for 30 min in a light-protected humidified chamber. The images were obtained with a laser scanning confocal microscope (Carl ZEISS, Germany). Superoxide production was demonstrated by red fluorescence labeling.

For quantification of ethidium fluorescence from endothelial cells, fluorescence (intensity × area) was measured only on the luminal side of the internal elastic lamina using the Image J in high-power (100×) images [19]. For each vessel, total fluorescence was calculated from three separate high-power fields taken in each section of the vessel to produce $n = 1$.

2.9. Measurement of 8-iso-prostaglandin F2α and serum amyloid A levels

Urine samples were collected from mice at the age of 12–16 weeks, and stored at −80 °C after addition of butyrated hydroxytoluene (BHT) at a final concentration of 0.01%. After purification using C18 reverse phase extraction column (Waters Corporation, MA), urine 8-*iso*-prostaglandin (PG) F2α levels were measured with EIA kits (Assay Designs Inc., MI) according to the manufacturer's instructions, and data were corrected by urine creatinine levels. Plasma samples were collected as above and stored at −80 °C after addition of BHT at a final concentration of 0.01%. We measured direct 8-*iso*-PGF2α levels from plasma samples with EIA kits (Assay Designs Inc., MI) according to the manufacturer's instructions.

We collected plasma from each mouse as shown in Section 2 and measured serum amyloid A (SAA) levels with mouse SAA ELISA kit (BioSource International Inc., CA) according to the manufacturer's instructions.

2.10. Statistical analysis

Data were expressed as mean ± S.E.M. One-way ANOVA was used to compare the differences among three groups with Fisher's PLSD test for post hoc analysis. Values of $P < 0.05$ were considered statistically significant.

Table 1
Effect of telmisartan on body weight, lipid contents, glucose and insulin levels, and vital signs

	Control	0.3 mg/kg	3 mg/kg
Female body weight (g)	21.8 ± 0.5	21.2 ± 0.3	21.2 ± 0.5
Male body weight (g)	26.9 ± 0.6	27.0 ± 0.4	26.7 ± 1.5
Total cholesterol (mg/dl)	478.6 ± 28.8	463.4 ± 19.1	464.9 ± 22.8
Triglyceride (mg/dl)	53.5 ± 6.8	50.0 ± 9.7	57.8 ± 8.1
HDL cholesterol (mg/dl)	9.4 ± 0.8	9.3 ± 0.9	9.0 ± 0.7
Glucose (mg/dl)	108.4 ± 8.2	116.1 ± 7.1	112.5 ± 5.5
Insulin (ng/ml)	0.24 ± 0.12	0.18 ± 0.06	0.24 ± 0.05
Heart rate (min^{-1})	543.9 ± 50.8	536.3 ± 89.7	540.5 ± 76.7
Systolic BP (mmHg)	107.4 ± 1.7	106.9 ± 2.1	90.1 ± 1.8*

Mice were fed a standard chow for 16 weeks and body weight of each mouse was measured. Mice were fasted for at least 12 h and bled, and plasma total cholesterol, triglyceride, high-density lipoprotein cholesterol, glucose and insulin levels were determined as described in Section 2 ($n = 8$ per group). Heart rate and systolic blood pressure were measured with the use of the tail-cuff method ($n = 15$ per group). Results were expressed as mean ± S.E.M.; BP, blood pressure.

* $P < 0.0001$ vs. control.

3. Results

3.1. The effects of telmisartan on blood pressure and plasma lipid levels

Body weight was not significantly different among three groups of each gender (Table 1). Neither plasma total cholesterol, triglyceride, nor high-density lipoprotein cholesterol levels were affected by the treatment with telmisartan. And neither plasma glucose, nor insulin levels were affected by the treatment with telmisartan. Although heart rate was not affected, 3 mg/kg telmisartan significantly reduced systolic blood pressure compared with that of control group (Table 1). In contrast, 0.3 mg/kg telmisartan did not change systolic blood pressure.

3.2. Atherosclerotic lesion formation at the aortic sinus

After feeding a standard chow for 16 weeks, the atherosclerotic lesion formation was assessed at the aortic sinus. Representative photographs of each mouse were shown in Fig. 1A. In quantitative analysis of histological examination with Sudan III staining, the atherosclerotic lesion formation of both 0.3 and 3 mg/kg groups were markedly reduced compared with control group in both gender (Fig. 1B). About plaque contents, scattered small fibrotic area was distributed in the plaque lesions of both control and telmisartan treatment groups when evaluated by Masson's trichrome staining (Fig. 2). MOMA-2-immunostained area was significantly reduced with telmisartan, but a ratio of positive-stained

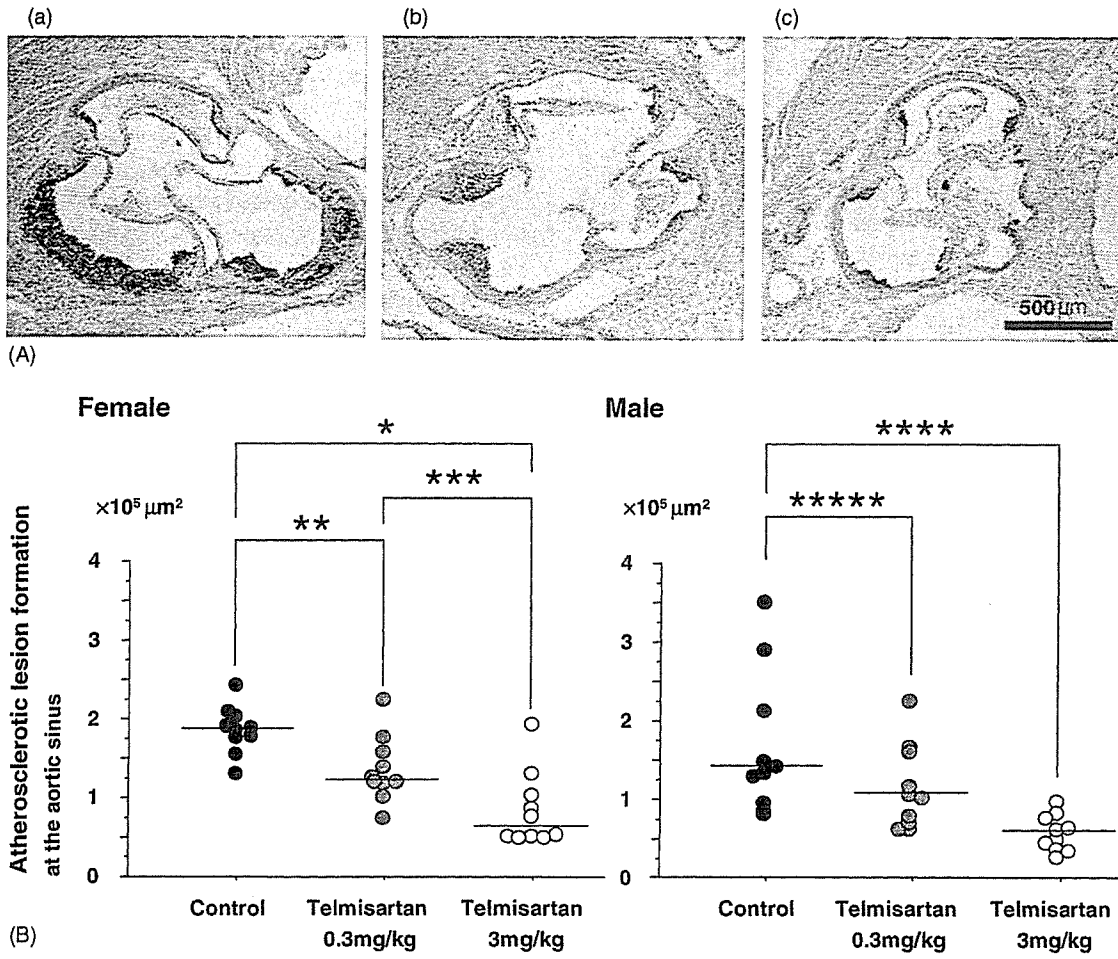

Fig. 1. (A) Representative photographs of atherosclerotic lesion formation at the aortic sinus of each mouse. Panel (a) through (c) are representative photographs of the atherosclerotic lesion formation at the aortic sinus of mice fed a standard chow in control group (a), that treated with 0.3 mg/kg telmisartan (b) and that treated with 3 mg/kg telmisartan (c), respectively. Sections were taken at the same level of aortic sinus and stained with Sudan III staining as described in Section 2. Original magnifications were 40×. A black bar on photomicrograph represents 500 μm. (B) Quantitative analysis of atherosclerotic lesion formation at the aortic sinus in both gender mice. The average lesion area of five sections at the aortic sinus from each mouse was quantified morphometrically as described in Section 2. Each symbol represents the average lesion area in each mouse, with the mean per group indicated by a horizontal line. After 12 weeks telmisartan treatment, the atherosclerotic lesion formation was significantly reduced in both 0.3 and 3 mg/kg telmisartan groups compared with control ($n = 10$ per group). $^{*}P < 0.0001$ vs. control; $^{**}P < 0.01$ vs. control; $^{***}P < 0.01$ vs. telmisartan 0.3 mg/kg; $^{****}P < 0.001$ vs. control; $^{*****}P < 0.05$ vs. control.

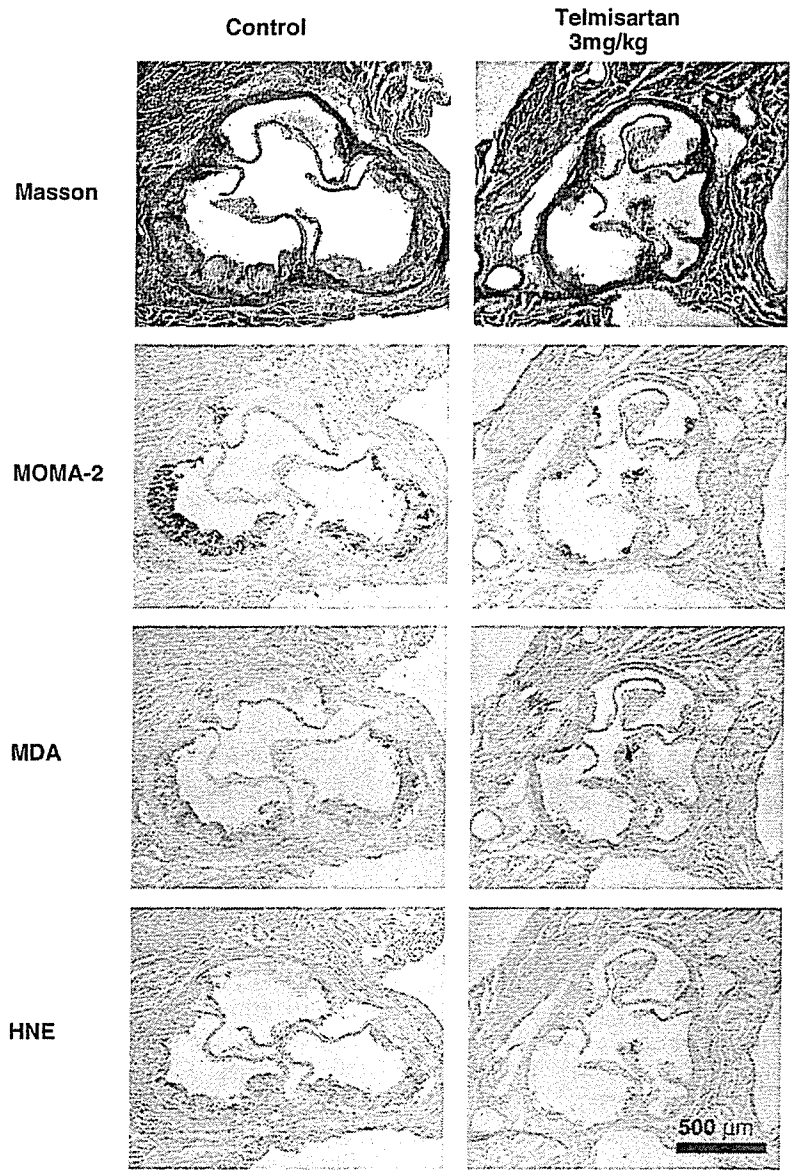

Fig. 2. Effect of telmisartan on plaque contents and the distribution of oxidative stress in atherosclerotic lesion at the aortic sinus. Panels are representative photographs of Masson trichrome staining and immunostained with MOMA-2, MDA and HNE in the atherosclerotic lesions from control group and 3 mg/kg telmisartan group (original magnification were 40×). Scattered fibrosis was partly distributed in the plaque lesions of both groups. On the whole, telmisartan reduced MOMA-2-, MDA- and HNE-immunostained areas compared with control group. A black bar on photomicrograph represents 500 μm.

area to total plaque area was not significantly different among three groups (data not shown). MDA-, HNE-immunostained areas were also reduced with telmisartan (Fig. 2).

3.3. Superoxide production from aortas

To investigate the effect of telmisartan on superoxide production in the aortic vessel wall, we measured superoxide production using the lucigenin-enhanced CL. By treatment with 0.3 and 3 mg/kg telmisartan, superoxide production was significantly decreased compared with control group (Fig. 3A).

3.4. NAD(P)H dependent oxidase activity of aorta homogenates

NAD(P)H dependent oxidase activity in aorta homogenates stimulated with 100 μM NADH or 100 μM NADPH was measured by use of the lucigenin-enhanced CL. Telmisartan significantly decreased NAD(P)H dependent oxidase activity by more than 60% in both 3 and 0.3 mg/kg groups compared with control group (Fig. 3B). Furthermore, aorta homogenates were incubated with either 100 μM DPI or 500 μM apocynin for 15 min to abolish the increment of NAD(P)H dependent oxidase activity. The addition of NAD(P)H oxidase inhibitors significantly reduced

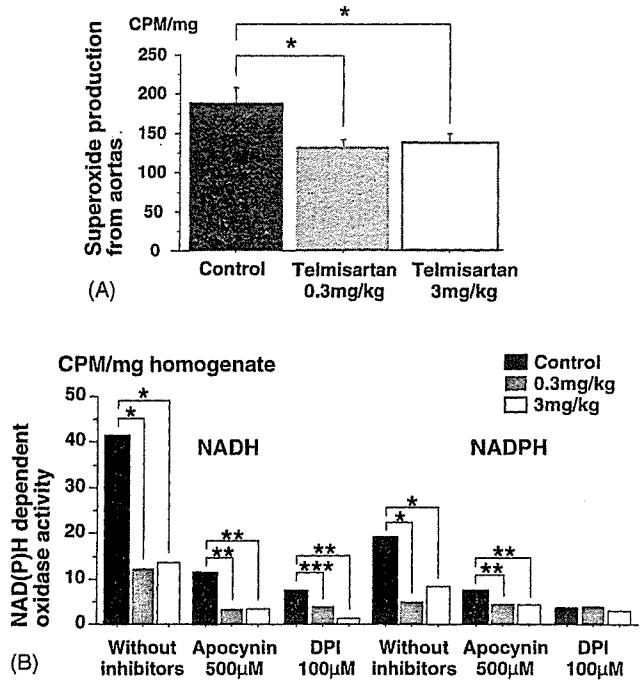

Fig. 3. (A) Effect of telmisartan on superoxide production from whole aortas using lucigenin-enhanced chemiluminescence. Aortic rings were incubated with the Cu–Zn superoxide dismutase inhibitor and vascular superoxide levels were measured by chemiluminescence with 10 μM lucigenin as described in Section 2. The counts by a luminometer were corrected by vessel dry weights. Results were expressed as mean ± S.E.M. ($n = 8$ per group). $^{*}P < 0.05$ vs. control. (B) Effect of telmisartan on NAD(P)H dependent oxidase activity of aorta homogenates using lucigenin-enhanced chemiluminescence. Aorta was homogenated and vascular NAD(P)H dependent oxidase activity was measured by use of chemiluminescence with 250 μM lucigenin in the presence of 100 μM NAD(P)H. NAD(P)H dependent oxidase activity was measured with 500 μM apocynin or 100 μM diphenylene iodinium (DPI) as described in Section 2. Results are expressed as mean ± S.E.M. of counts by luminometer in each group ($n = 8$ per group). $^{*}P < 0.0001$ vs. control; $^{**}P < 0.001$ vs. control; $^{***}P < 0.05$ vs. control.

lucigenin-enhanced CL in both control and telmisartan treatment groups.

3.5. *In situ superoxide production in the vessel wall of aorta*

In situ superoxide production was measured using DHE oxidative fluorescent microtopography. Ethidium fluorescence was detected throughout all layers of the vessel wall and both doses (0.3 and 3 mg/kg) of telmisartan significantly suppressed the staining (Fig. 4A). We next focused on the vascular superoxide production in the endothelial cells by measuring the ethidium fluorescence particularly on the luminal side of the internal elastic lamina. Endothelial ethidium fluorescence in 0.3 mg/kg group was decreased by 30% compared with control group and by 40% in 3 mg/kg group (Fig. 4B). These results indicated that telmisartan decreased superoxide production from the vessel wall, particularly from endothelial cells.

3.6. *8-iso-PGF2α and SAA levels*

8-*iso*-PGF2α level was measured as an indicative marker of systemic oxidative stress. 8-*iso*-PGF2α levels from both urine (Fig. 5A) and plasma samples (Fig. 5B) were significantly decreased with telmisartan treatment compared with control group. On the other hand, SAA levels did not change by telmisartan (Fig. 5C).

4. Discussion

In the present study, we demonstrated that telmisartan suppressed the atherosclerotic lesion formation in apoE-KO mice. The suppressive effect was detected by 0.3 mg/kg telmisartan, which did not change systolic blood pressure, and further suppression occurred by 3 mg/kg telmisartan. As the mechanism of the drug's anti-atherogenic action, we focused on the effects for oxidative states in vivo and in vitro. Telmisartan reduced MDA- and HNE-immunostained areas compared with control group. Telmisartan suppressed superoxide production from the vessel wall via reducing NAD(P)H dependent oxidase activity. Telmisartan also reduced 8-*iso*-PGF2α levels in urine and plasma samples, which are one of indices of systemic oxidative stress. These inhibitory effects on oxidative stress were associated with suppression of atherosclerotic lesion formation.

Several animal studies demonstrated that ARB showed anti-atherogenic effects besides its effect on blood pressure [10–13]. Our finding is in agreement with the results of Hayak et al. and Dol et al., in which ARB reduced atherosclerotic lesion formation in apoE-KO mice via decreased chemokine expression and macrophage accumulation, and the inhibition of LDL oxidation [11,12]. In the present study, we demonstrated that telmisartan reduced atherosclerotic lesion formation in association with the suppression of oxidative stress via the inhibition of NAD(P)H oxidase activity.

Ang II stimulation has been reported to produce ROS from various vascular cell types [2–4]. ROS from the vessel wall are thought to play critical roles in atherogenesis. ROS induce the expression of adhesion molecules and chemokines, accelerate the formation of atherosclerotic plaque, increase matrix metalloprotease production and cause the vulnerable changes of fibrous cap [20].

In the present study, we clearly demonstrated that telmisartan suppressed superoxide production from the vessel wall assessed by lucigenin-enhanced CL method. This action was independent of the blood pressure lowering effect. We also revealed the inhibitory action of telmisartan on superoxide production by DHE staining. Telmisartan suppressed superoxide signals in all layers of aortas, particularly in the endothelium. We next focused on NAD(P)H oxidase to clarify the mechanisms of suppression of superoxide production. Superoxide anion is produced via the activation of NAD(P)H oxidase in vessel wall cells and plays an important role as the intracellular transmission factor in the Ang

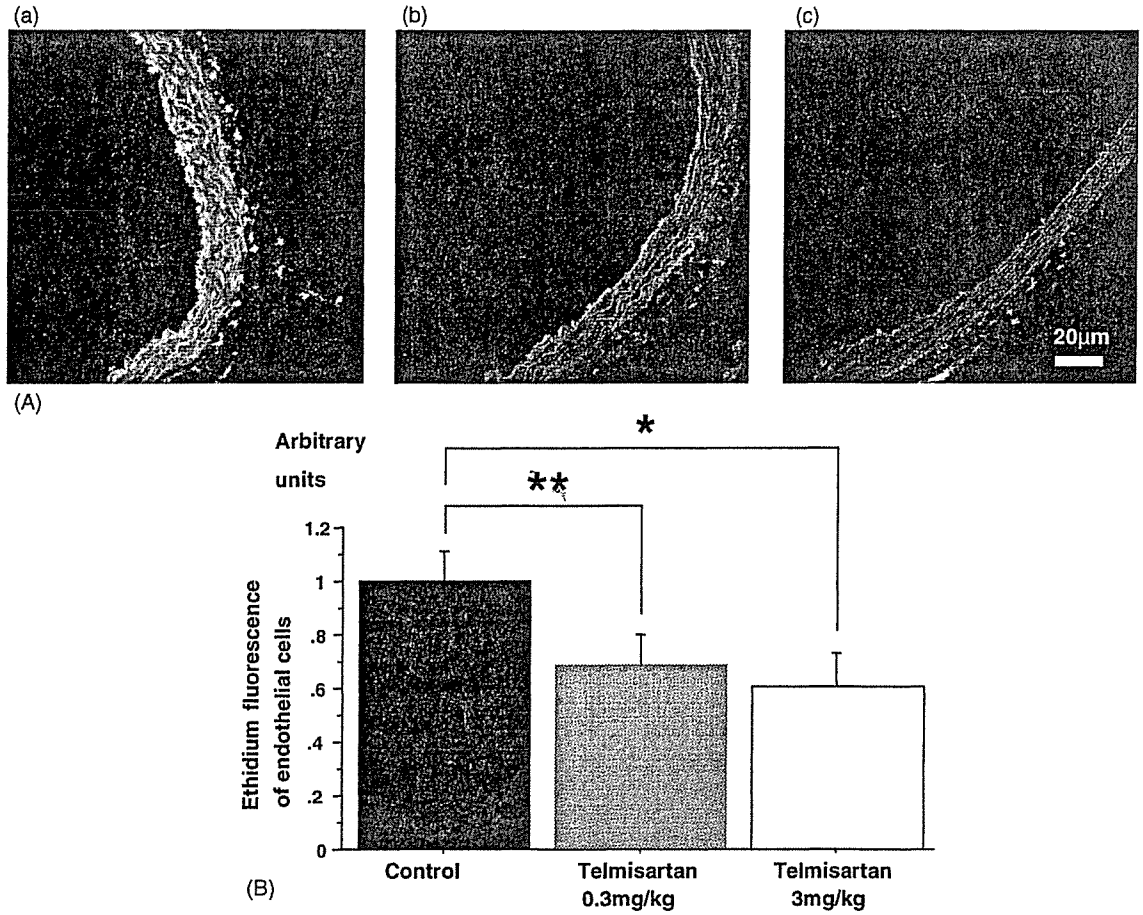

Fig. 4. (A) Representative photographs of in situ superoxide production in aortic vessel wall using dihydroethidium staining. Panel (a) through (c) are representative photographs of aortic vessel wall from each mouse in control group (a), that treated with 0.3 mg/kg telmisartan (b) and that treated with 3 mg/kg telmisartan (c), respectively. Sections were stained with dihydroethidium as described in Section 2. Original magnification were 200×. A white bar represents 20 μm. (B) Quantitative analysis of in situ superoxide production in aorta endothelial cells using dihydroethidium staining. For quantification of ethidium fluorescence from the endothelial cells in high-power (200×) images, fluorescence (intensity × area) was measured only on the luminal side of the internal elastic lamina using the Image J as described in Section 2 and expressed in arbitrary units. Results were expressed as mean ± S.E.M. in each group ($n = 10$ per group). $^{*}P < 0.05$ vs. control; $^{**}P = 0.07$ vs. control.

II-signaling system [21]. Ang II-mediated hypertension is associated with the increased superoxide production and NAD(P)H oxidase activity [7]. Other than hypertension, the increased superoxide production due to NAD(P)H oxidase activation was demonstrated in the rabbit model of atherosclerosis [22]. We examined lucigenin-enhanced CL with NAD(P)H as the substrates and revealed that telmisartan suppressed NAD(P)H dependent oxidase activity with the dosage that did not change blood pressure. This effect was reduced by DPI, an inhibitor of all flavoenzymes and also by apocynin, a more specific inhibitor for NAD(P)H oxidase. These results indicated that the increment of superoxide production was reduced by inactivation of NAD(P)H dependent oxidase activity due to Ang II type 1 receptor blockade with telmisartan.

Our findings are in accordance with the study of Warnholtz et al., who showed that Bay 10-6734, an ARB, reduced plaque formation in association with reductions of vascular superoxide production and NAD(P)H oxidase activity in the rabbit model of atherosclerosis [22]. They did not show whether the anti-atherogenic effects of Bay 10-6734 were independent of the blood pressure lowering effect. In the present study, we clearly demonstrated that telmisartan, a clinically used ARB, reduced atherosclerotic lesion formation without changing blood pressure in apoE-KO mice. In most animal studies showing the blood pressure-independent anti-atherogenic actions of ARB, the far-high dosages have been used compared with those applied clinically [10–13]. In the present study, we showed that the anti-atherogenic action of telmisartan was detected with 0.3 mg/kg, which is lower than the clinically relevant dose. We also showed that telmisartan reduced not only vascular superoxide production but also the marker of systemic oxidative status. 8-*iso*-PGF2α has been recognized as a marker of systemic oxidative stress [23] and revealed as a risk marker in patients with coronary heart disease in matched case-control studies [24]. In this study, telmisartan suppressed 8-*iso*-PGF2α levels in both urine and plasma with the non-blood pressure lowing dosage.

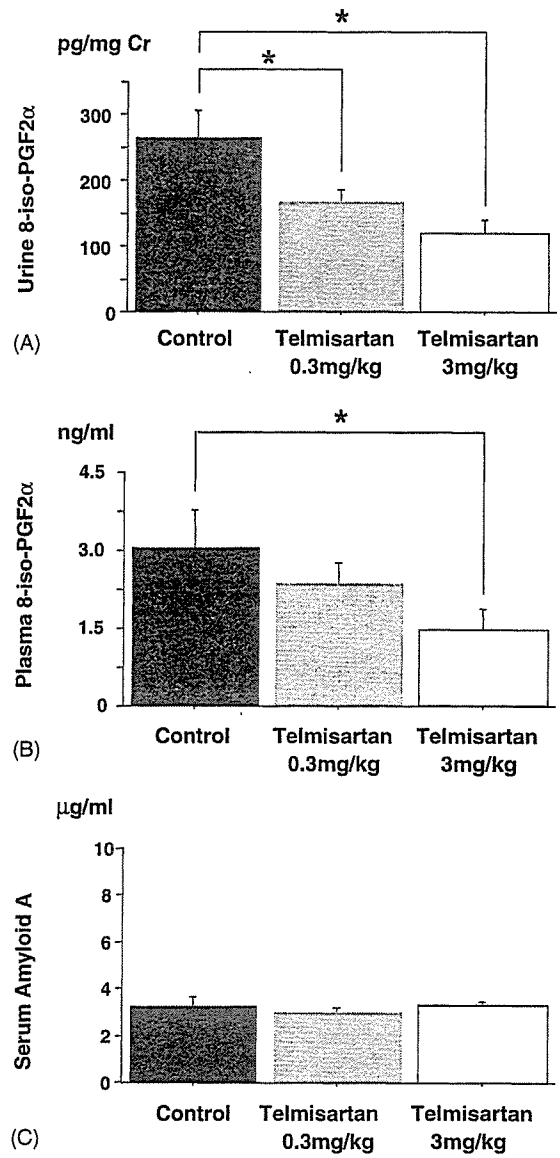

Fig. 5. (A) and (B) Effect of telmisartan on 8-*iso*-PGF2α levels of urine and plasma samples 8-*iso*-PGF2α from urine (A) and plasma (B) samples were measured as described in Section 2. Urine data are corrected by urine creatinine levels. Results were expressed as mean ± S.E.M. ($n = 8$ per group). $^{*}P < 0.05$ vs. control. (C) Effect of telmisartan on SAA levels. SAA levels were measured as described in Section 2. Results were expressed as mean ± S.E.M. ($n = 8$ per group).

The association of suppressed oxidative stress and reduction of atherosclerotic lesion formation does not necessarily mean the cause-effect relation. Both occurred independently of changes in blood pressure, and the well-known roles of oxidative stress in the initiation and progression of atherosclerosis strongly suggest that the anti-oxidative effects are at least partly responsible for the suppression of atherosclerotic lesion formation by telmisartan. Telmisartan might, however, reduce atherosclerotic lesion size by mechanisms other than its effects on oxidative stress, such as anti-inflammatory effects and effects on peroxisome proliferator-activated receptor-gamma (PPAR-g) activity. It is reported that telmisartan induced PPAR-g activation [25,26], but in the present study, telmisartan did not change plasma glucose, triglyceride or insulin levels. Therefore the effect of telmisartan on PPAR-g seemed to play a minimum role in the present study. Further, Ang II increases expression of lectin-like oxidized LDL receptor of macrophage and accelerates the foam cell formation and the deposition of oxidized lipid to the plaque [27]. Further studies are needed to clarify how inhibition of those actions of Ang II by telmisartan is related to its anti-atherogenic action.

As a limitation of the present study, we quantified superoxide production from aorta homogenates by use of 250 μm lucigenin. The validity of data on superoxide has been questioned when the relatively high dose of lucigenin is applied. In the present study, however, the levels of oxidative stress were relatively low, and we could not detect any fluorescence signals when we used 5 μm lucigenin, which was revealed not to produce superoxide by itself. In the report of Warnholtz et al., they compared the data on superoxide productions measured by 5 μM lucigenin with those by 250 μM lucigenin and confirmed the validity of the data obtained by the latter concentration [22].

In conclusion, we for the first time reported that in apoE-KO mice clinically relevant doses of telmisartan reduced atherosclerosis in association with suppressions in vascular oxidative stress and vascular systemic oxidative state. Our results suggest that telmisartan is beneficial not only for hypertension but also for atherosclerosis and imply that this drug may work as an anti-oxidant in various organs, although additional experiments will be needed.

References

[1] Daugherty A, Cassis L. Chronic angiotensin II infusion promotes atherogenesis in low density lipoprotein receptor −/− mice. Ann NY Acad Sci 1999;892:108–18.
[2] Zhang H, Schmeisser A, Garlichs CD, et al. Angiotensin II-induced superoxide anion generation in human vascular endothelial cells: role of membrane-bound NADH/NADPH-oxidases. Cardiovasc Res 1999;44:215–22.
[3] Sorescu D, Weiss D, Lassegue B, et al. Superoxide production and expression of nox family proteins in human atherosclerosis. Circulation 2002;105:1429–35.
[4] Cathcart MK. Regulation of superoxide anion production by NADPH oxidase in monocytes/macrophages: contributions to atherosclerosis. Arterioscler Thromb Vasc Biol 2004;24:23–8.
[5] Diet F, Pratt RE, Berry GJ, Momose N, Gibbons GH, Dzau VJ. Increased accumulation of tissue ACE in human atherosclerotic coronary artery disease. Circulation 1996;94:2756–67.
[6] Yang BC, Phillips MI, Mohuczy D, et al. Increased angiotensin II type 1 receptor expression in hypercholesterolemic atherosclerosis in rabbits. Arterioscler Thromb Vasc Biol 1998;18:1433–9.
[7] Rajagopalan S, Kurz S, Munzel T, et al. Angiotensin II-mediated hypertension in the rat increases vascular superoxide production via membrane NADH/NADPH oxidase activation. Contribution to alterations of vasomotor tone. J Clin Invest 1996;97:1916–23.
[8] Chen XL, Tummala PE, Olbrych MT, Alexander RW, Medford RM. Angiotensin II induces monocyte chemoattractant protein-1 gene expression in rat vascular smooth muscle cells. Circ Res 1998;83:952–9.

[9] Tummala PE, Chen XL, Sundell CL, et al. Angiotensin II induces vascular cell adhesion molecule-1 expression in rat vasculature: a potential link between the renin-angiotensin system and atherosclerosis. Circulation 1999;100:1223–9.
[10] Strawn WB, Chappell MC, Dean RH, Kivlighn S, Ferrario CM. Inhibition of early atherogenesis by losartan in monkeys with diet-induced hypercholesterolemia. Circulation 2000;101:1586–93.
[11] Hayek T, Attias J, Coleman R, et al. The angiotensin-converting enzyme inhibitor, fosinopril, and the angiotensin II receptor antagonist, losartan, inhibit LDL oxidation and attenuate atherosclerosis independent of lowering blood pressure in apolipoprotein E-deficient mice. Cardiovasc Res 1999;44:579–87.
[12] Dol F, Martin G, Staels B, et al. Angiotensin AT1 receptor antagonist in apolipoprotein E-deficient mice. J Cardiovasc Pharmacol 2001;38:395–405.
[13] Takai S, Kim S, Sakonjo H, Miyazaki M. Mechanisms of angiotensin II type 1 receptor blocker for anti-atherosclerotic effect in monkeys fed a high-cholesterol diet. J Hypertens 2003;21:361–9.
[14] Paigen B, Morrow A, Holmes PA, Mitchell D, Williams RA. Quantitative assessment of atherosclerotic lesions in mice. Atherosclerosis 1987;68:231–40.
[15] Ozaki M, Kawashima S, Yamashita T, et al. Overexpression of endothelial nitric oxide synthase accelerates atherosclerotic lesion formation in apoE-deficient mice. J Clin Invest 2002;110:331–40.
[16] Bradford MM. A rapid and sensitive method for the quantification of microgram quantities of protein utilizing the principle of protein-dye binding. Anal Biochem 1972;72:248–54.
[17] Munzel T, Kurz S, Rajagopalan S, et al. Hydralazine prevents nitroglycerin tolerance by inhibiting activation of a membrane-bound NADH oxidase: a new action for an old drug. J Clin Invest 1996;98:1465–70.
[18] Miller FJ, Gutterman DD, Rios CD, Heistad DD, Davidson BL. Superoxide production in vascular smooth muscle contributes to oxidative stress and impaired relaxation in atherosclerosis. Circ Res 1998;82:1298–305.
[19] Alp NJ, Mussa S, Khoo J, et al. Tetrahydrobiopterin-dependent preservation of nitric oxide-mediated endothelial function in diabetes by targeted transgenic GTP-cyclohydrolase I overexpression. J Clin Invest 2003;112:725–35.
[20] Rajagopalan S, Meng XP, Ramasamy S, Harrison DG, Galis ZS. Reactive oxygen species produced by macrophage-derived foam cells regulate the activity of vascular matrix metalloproteinases in vitro. Implications for atherosclerotic plaque stability. J Clin Invest 1996;98:2572–9.
[21] Cai H, Harrison DG. Endothelial dysfunction in cardiovascular diseases: the role of oxidative stress. Circ Res 2000;87:840–4.
[22] Warnholtz A, Nickenig G, Schulz E, et al. Increased NADH-oxidase-mediated superoxide production in the early stages of atherosclerosis: evidence for involvement of the renin-angiotensin system. Circulation 1999;99:2027–33.
[23] Pratico D, Tangirala RK, Rader DJ, Rokach J, FitzGerald GA. Vitamin E suppresses isoprostane generation in vivo and reduces atherosclerosis in ApoE-deficient mice. Nat Med 1998;4:1189–92.
[24] Schwedhelm E, Bartling A, Lenzen H, et al. Urinary 8-*iso*-prostaglandin F2alpha as a risk marker in patients with coronary heart disease: a matched case-control study. Circulation 2004;109:843–8.
[25] Schupp M, Janke J, Clasen R, Unger T, Kintscher U. Angiotensin type 1 receptor blockers induce peroxisome proliferator-activated receptor-gamma activity. Circulation 2004;109:2054–7.
[26] Benson SC, Pershadsingh HA, Ho CI, et al. Identification of telmisartan as a unique angiotensin II receptor antagonist with selective PPAR gamma-modulating activity. Hypertension 2004;43:993–1002.
[27] Sawamura T, Kume N, Aoyama T, et al. An endothelial receptor for oxidized low-density lipoprotein. Nature 1997;386:73–7.

Stoichiometric Relationships Between Endothelial Tetrahydrobiopterin, Endothelial NO Synthase (eNOS) Activity, and eNOS Coupling in Vivo

Insights From Transgenic Mice With Endothelial-Targeted GTP Cyclohydrolase 1 and eNOS Overexpression

Jennifer K. Bendall, Nicholas J. Alp, Nicholas Warrick, Shijie Cai, David Adlam, Kirk Rockett, Mitsuhiro Yokoyama, Seinosuke Kawashima, Keith M. Channon

Abstract—Endothelial dysfunction in vascular disease states is associated with reduced NO bioactivity and increased superoxide ($O_2^{\cdot-}$) production. Some data suggest that an important mechanism underlying endothelial dysfunction is endothelial NO synthase (eNOS) uncoupling, whereby eNOS generates $O_2^{\cdot-}$ rather than NO, possibly because of a mismatch between eNOS protein and its cofactor tetrahydrobiopterin (BH4). However, the mechanistic relationship between BH4 availability and eNOS coupling in vivo remains undefined because no studies have investigated the regulation of eNOS by BH4 in the absence of vascular disease states that cause pathological oxidative stress through multiple mechanisms. We investigated the stoichiometry of BH4–eNOS interactions in vivo by crossing endothelial-targeted eNOS transgenic (eNOS-Tg) mice with mice overexpressing endothelial GTP cyclohydrolase 1 (GCH-Tg), the rate-limiting enzyme in BH4 synthesis. eNOS protein was increased 8-fold in eNOS-Tg and eNOS/GCH-Tg mice compared with wild type. The ratio of eNOS dimer:monomer was significantly reduced in aortas from eNOS-Tg mice compared with wild-type mice but restored to normal in eNOS/GCH-Tg mice. NO synthesis was elevated by 2-fold in GCH-Tg and eNOS-Tg mice but by 4-fold in eNOS/GCH-Tg mice compared with wild type. Aortic BH4 levels were elevated in GCH-Tg and maintained in eNOS/GCH-Tg mice but depleted in eNOS-Tg mice compared with wild type. Aortic and cardiac $O_2^{\cdot-}$ production was significantly increased in eNOS-Tg mice compared with wild type but was normalized after NOS inhibition with *N*ω-nitro-L-arginine methyl ester hydrochloride (L-NAME), suggesting $O_2^{\cdot-}$ production by uncoupled eNOS. In contrast, in eNOS/GCH-Tg mice, $O_2^{\cdot-}$ production was similar to wild type, and L-NAME had no effect, indicating preserved eNOS coupling. These data indicate that eNOS coupling is directly related to eNOS–BH4 stoichiometry even in the absence of a vascular disease state. Endothelial BH4 availability is a pivotal regulator of eNOS activity and enzymatic coupling in vivo. (***Circ Res.* 2005;97:864-871.**)

Key Words: endothelial nitric oxide synthase ■ tetrahydrobiopterin ■ nitric oxide ■ superoxide

Nitric oxide (NO), produced by endothelial NO synthase (eNOS) in the vascular endothelium, is a critical signaling molecule in vascular homeostasis.[1] NO serves as an endothelium-derived relaxing factor, regulates vasomotor tone and blood pressure,[1,2] and has multiple antiatherogenic roles by inhibiting vascular smooth muscle cell proliferation, platelet aggregation, and leukocyte adhesion.[1] Loss of NO bioavailability is a key feature of endothelial dysfunction in vascular disease states such as hypertension, diabetes, and atherosclerosis. Furthermore, impaired NO-mediated endothelial function is an independent risk factor for cardiovascular disease.[3–5] Several factors contribute to loss of NO bioavailability, including reduced NO synthesis and NO scavenging by reactive oxygen species (ROS).[6] Under physiological conditions, there is a balance between endothelial NO and ROS production. However, vascular diseases are associated with increased ROS generation.[6] Several oxidase systems contribute to the increased oxidative stress, notably the NADPH oxidases.[7,8]

Increasing evidence suggests that eNOS itself can generate superoxide ($O_2^{\cdot-}$) under certain pathophysiological conditions.[9] Ozaki et al[10] reported recently that transgenic overexpression of eNOS in apolipoprotein E knockout mice paradoxically increases vascular $O_2^{\cdot-}$ production because of

Original received March 9, 2005; revision received August 10, 2004; accepted September 12, 2005.

From the Department of Cardiovascular Medicine (J.K.B., N.J.A., N.W., S.C., D.A., K.M.C.), University of Oxford, John Radcliffe Hospital, United Kingdom; Childhood Infection Group (K.R.), Wellcome Trust Centre for Human Genetics, University of Oxford, United Kingdom; and Kobe University School of Medicine (M.Y., S.K.), Japan.

Correspondence to Professor Keith M. Channon, Department of Cardiovascular Medicine, John Radcliffe Hospital, Oxford, OX3 9DU, UK. E-mail keith.channon@cardiov.ox.ac.uk

Circulation Research is available at http://circres.ahajournals.org DOI: 10.1161/01.RES.0000187447.03525.72

enzymatic uncoupling of increased eNOS protein levels. Recent data indicate that the pterin cofactor tetrahydrobiopterin (BH4) is a major determinant of whether eNOS produces NO or $O_2^{\cdot-}$.[11,12] When BH4 levels are insufficient, there is a shift toward the production of $O_2^{\cdot-}$ as electron transfer within the active site of eNOS becomes uncoupled from L-arginine oxidation, and molecular oxygen is instead reduced to form $O_2^{\cdot-}$.[11] $O_2^{\cdot-}$ generated by eNOS has been implicated in endothelial dysfunction associated with a number of vascular disease states, including diabetes, smoking, hypertension, and atherosclerosis,[10,12-16] and BH4 supplementation improves endothelium-dependent vasodilatation under these conditions.[16] However, the effects of systemic pharmacological BH4 supplementation in these studies may be mediated in part by nonspecific antioxidant properties of acute high-dose BH4,[17] which can increase NO bioavailability indirectly by reducing its scavenging by ROS.

Recent studies have focused on the potential role of BH4 oxidation, to dihydrobiopterin (BH2) and other biopterin species, in reducing BH4 bioavailability in preatherosclerotic disease states.[16-18] In particular, the interaction of BH4 with peroxynitrite (generated from the reaction between NO and $O_2^{\cdot-}$) rapidly oxidizes BH4 and can provoke eNOS uncoupling and endothelial dysfunction.[12,19-21] Indeed, eNOS uncoupling may exacerbate the process by contributing to BH4 oxidation. However, it is unclear whether eNOS uncoupling alone is sufficient to initiate BH4 oxidation and exacerbate eNOS uncoupling in vivo because all in vivo studies to date have evaluated BH4-dependent eNOS regulation in complex vascular disease states in which multiple inflammatory and redox pathways are implicated. Other previous studies of the role of BH4 in eNOS function have relied on purified recombinant proteins in reconstituted cell-free systems.[9,11,22,23]

Accordingly, we sought to investigate the importance of BH4 in regulating eNOS activity in vivo in healthy animals without vascular disease. We used a transgenic mouse model with endothelial-targeted overexpression of GTP cyclohydrolase 1 (GTPCH), the rate-limiting enzyme in BH4 synthesis, in which endothelial BH4 levels are specifically increased.[24] We crossed this transgenic mouse with a mouse overexpressing eNOS in the endothelium to generate mouse models with graded alterations in endothelial BH4 and eNOS levels to investigate the mechanistic relationships between BH4 and eNOS coupling in vivo.

Materials and Methods

Animals

All studies involving laboratory animals were conducted in accordance with the UK Home Office Animals (Scientific Procedures) Act 1986 (HMSO, UK). eNOS transgenic (eNOS-Tg) mice, in which bovine eNOS transgene overexpression is targeted to the vascular endothelium under the control of the murine preproendothelin-1 promoter in a C57BL/6 background, were produced as described previously.[25] GTPCH transgenic (GCH-Tg) mice, in which human GTPCH transgene overexpression is targeted to the endothelium under control of the murine Tie-2 promoter, were generated in a C57BL/6 background as described previously.[26] Heterozygote eNOS-Tg mice were mated with heterozygote GCH-Tg mice to produce experimental eNOS/GCH-Tg, eNOS-Tg, GCH-Tg, and wild-type littermates in a 1:1:1:1 ratio. Mice (between 13 and 20 weeks of age in all experiments) were housed in individually ventilated cages with 12-hour light/dark cycle and controlled temperature (20°C to 22°C) and fed normal chow and water ad libitum.

Western Blot Analysis

Lung samples ($n \geq 4$ per group) were homogenized on ice for 20 seconds in lysis buffer (50 mmol/L Tris, pH 7.5, 150 mmol/L NaCl, 0.1% SDS, 0.5% deoxycholate, 1% Nonidet P-40) containing protease inhibitors (Complete; Boehringer Mannheim) and 1 mmol/L phenylmethylsulfonyl fluoride. Protein lysates (8 μg) were resolved using SDS-PAGE and transferred to polyvinylidene difluoride membranes. Membranes were incubated with a 1:2000 dilution of mouse anti-eNOS monoclonal antibody (Transduction Laboratories), which recognizes murine and bovine eNOS, followed by a 1:2500 dilution of rabbit anti-mouse horseradish peroxidase–conjugated secondary antibody (Promega). Protein bands were visualized by chemiluminescence. To investigate the ratio of eNOS homodimer to monomer, Western blots were performed as above using nonboiled aortic lysates and low-temperature SDS-PAGE as described previously.[27]

Primary Cultures of Murine Lung Endothelial Cells

Lungs were harvested into culture medium (35% DMEM, 35% Ham's F-10 nutrient mixture, 20% FBS, 2 mmol/L L-glutamine, 100 U/100 μg/mL penicillin–streptomycin, 100 μg/mL heparin, and 50 μg/mL endothelial mitogen [Biogenesis]), cut into 1- to 2-mm pieces and digested using 0.1% collagenase type I for 1 hour at 37°C. The lung digest was passed through a 100-μm cell strainer. Cells were centrifuged, resuspended in culture medium, and plated onto 0.1% gelatin-coated cover slips. Cultures were maintained at 37°C in humidified 5% CO_2/95% air atmosphere for 72 hours before fixation with 4% paraformaldehyde.

Immunocytochemistry

Fixed cultures were permeabilized with PBS containing 0.5% Triton X-100, and nonspecific staining was reduced by blocking with 10% normal goat serum. Cultures were incubated with a polyclonal rabbit anti-eNOS primary antibody (Transduction Laboratories) followed by goat anti-rabbit secondary antibody (Alexa Fluor 488; Molecular Probes). Cells were mounted with cover slips using Vectashield containing propidium iodide (Vector Laboratories) and imaged using a Bio-Rad MRC-1024 laser-scanning confocal microscope.

Measurement of Biopterins and Neopterin

Biopterins, such as BH4, BH2 and biopterin, and neopterin were measured in aortic homogenates by high-performance liquid chromatography (HPLC) analysis after iodine oxidation in acidic or alkaline conditions as described previously.[24,28] In brief, thoracic aortas ($n=6$ to 8 per group) were homogenized for 20 seconds in ice-cold extract buffer (50 mmol/L Tris-HCl, pH 7.4, 1 mmol/L dithiothreitol, and 1 mmol/L EDTA) containing 0.1 μmol/L neopterin as an internal recovery standard. Samples were deproteinated before undergoing oxidation with 1% iodine/2% potassium iodide under either acidic or basic conditions. Biopterin content was assessed using HPLC in 5% methanol/95% water using an ACE 5 C18 column (ACT) and fluorescence detection (350 nm excitation and 450 nm emission). BH4 concentration was calculated as picomoles per milligram of protein by subtracting BH2 and biopterin from total biopterin content.

Arginine-to-Citrulline Conversion

NOS enzymatic activity, and indirectly NO synthesis, was measured by the conversion of ^{14}C L-arginine to ^{14}C L-citrulline in fresh intact aorta ($n=5$ to 8 per group) and lung homogenate ($n=6$ per group) as described previously.[24,29] The integrals of citrulline peaks were expressed as a proportion of total ^{14}C counts for each sample.

Electron Paramagnetic Resonance Spectroscopy

Electron paramagnetic resonance (EPR) spectroscopy was used to quantify vascular NO production according to previously described and validated methods.[30] In brief, freshly harvested aortas (n=8 to 11 per group) were stimulated with calcium ionophore (A23187; 1 μmol/L) in 100 μL Krebs–HEPES buffer, then incubated with colloid iron (II) diethyldithiocarbamate [Fe(DETC)$_2$] (285 μmol/L) at 37°C for 90 minutes. After incubation, aortas were snap-frozen in a column of Krebs–HEPES buffer in liquid nitrogen, and EPR spectra were obtained using an X-band EPR spectrometer (Miniscope MS 200; Magnettech). Signals were quantified by measuring the total amplitude, after correction of baseline, and after subtracting background signals from incubation with colloid Fe(DETC)$_2$ alone.

Lucigenin-Enhanced Chemiluminescence Detection of Superoxide in Heart Lysates

Basal $O_2^{\cdot-}$ production was measured in left ventricular (LV) homogenates (n=7 to 10 per group) using the technique of lucigenin (5 μmol/L) chemiluminescence according to methods described previously.[14,31] In brief, hearts were flushed with ice-cold Krebs–HEPES buffer, the LV excised, and snap-frozen in liquid nitrogen. Samples were homogenized in Kreb–HEPES buffer containing protease inhibitors (Complete; Boehringer Mannheim) at pH 7.4. Chemiluminescence was measured in a FB12 luminometer (Berthold Detection Systems) at 37°C. Chemiluminescence of 200 μg LV protein was recorded every minute for 8 minutes. The NOS inhibitor *N*ω-nitro-L-arginine methyl ester hydrochloride (L-NAME; 1 mmol/L) was subsequently added and chemiluminescence recorded for an additional 5 minutes. Background readings were subtracted from sample readings and results expressed as counts per second.

Lucigenin-Enhanced Chemiluminescence Detection of Superoxide in Intact Aorta

Basal $O_2^{\cdot-}$ production was measured in intact aorta (n=8 to 12 per group) according to methods described previously.[14,32] In brief, freshly cleaned and harvested thoracic aortas were opened longitudinally, cut into 2, and transferred to ice-cold Krebs–HEPES buffer. Vessels were equilibrated in Krebs–HEPES buffer gassed with 95% oxygen/5% carbon dioxide for 30 minutes at 37°C, with one half of each vessel being incubated in the presence of L-NAME (1 mmol/L). Lucigenin (20 μmol/L) chemiluminescence was then recorded every minute for 10 minutes as above. Background readings were subtracted from sample readings and results expressed as counts per second per milligram dry weight of aorta.

Oxidative Fluorescent Microtopography

$O_2^{\cdot-}$ production in tissue sections of mouse aorta (n=5 to 7 per group) was detected using the fluorescent probe dihydroethidium (DHE), as described previously.[14,24,33] Fresh segments of thoracic aorta were frozen in optimal cutting temperature compound. Cryosections (30 μm) were incubated with Krebs–HEPES buffer with or without L-NAME (1 mmol/L; to inhibit eNOS) for 30 minutes at 37°C, then for an additional 5 minutes with DHE (2 μmol/L; Molecular Probes). Images were obtained using a Bio-Rad laser-scanning confocal microscope, equipped with a krypton/argon laser, using identical acquisition settings for each section. DHE fluorescence was quantified by automated image analysis using Image-Pro Plus software (Media Cybernetics). DHE fluorescence from high power (×60) images was measured only on the luminal side of the internal elastic lamina to quantify endothelial cell fluorescence. For each vessel, mean fluorescence was calculated from 4 separate high-power fields taken in each quadrant of the vessel to produce n=1, and all experiments were performed in a batch design.

Statistical Analysis

One-way ANOVA tests were used to compare data sets, with appropriate post hoc correction for multiple comparisons. $P<0.05$ was considered significant. Data are expressed as means and SEM.

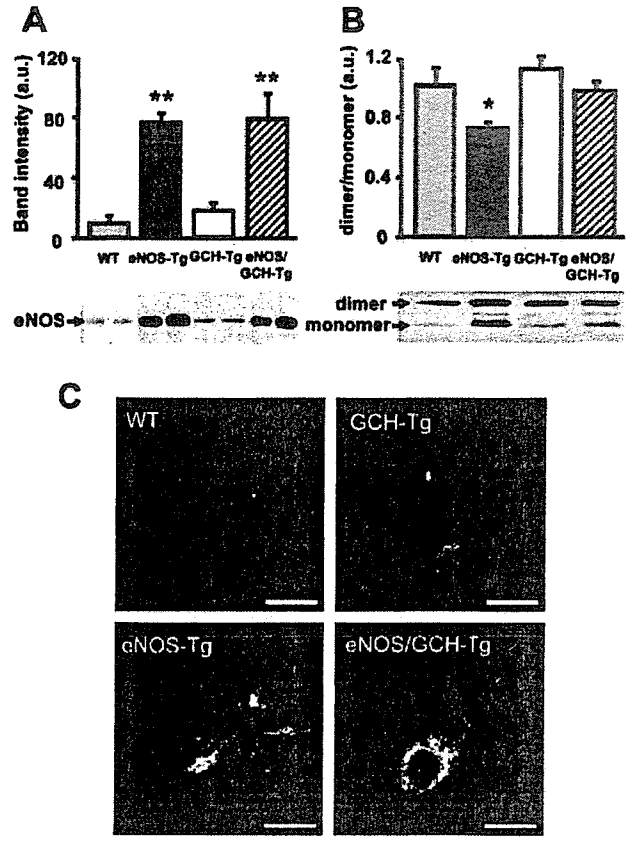

Figure 1. Immunoblotting with a murine anti-eNOS monoclonal antibody to detect native and transgenic eNOS monomer protein in boiled lung lysates (A) and eNOS dimer:monomer protein bands in aortic lysates from wild-type (WT), eNOS-Tg, GCH-Tg, and eNOS/GCH-Tg mice (B); n=4 animals per group; *$P<0.05$ and **$P<0.001$ compared with WT. a.u. indicates arbitrary units. C, Immunofluorescent detection of eNOS (green), counterstained with propidium iodide (red), in primary endothelial cells cultured from WT, eNOS-Tg, GCH-Tg, and eNOS/GCH-Tg mice. Bar=20 μm.

Results

eNOS Protein Levels and Subcellular Localization

Western blot analysis confirmed that eNOS protein levels were elevated 8-fold in eNOS-Tg compared with wild-type animals ($P<0.001$; Figure 1A). Overexpression of endothelial GTPCH, the rate-limiting enzyme in BH4 synthesis, in GCH-Tg mice did not significantly alter eNOS protein levels compared with wild type. However, as for eNOS-Tg mice, eNOS protein levels were elevated 8-fold in double-transgenic eNOS/GCH-Tg mice.

We used low-temperature SDS-PAGE and immunoblotting to investigate eNOS homodimerization and the ratio of eNOS dimer to monomer in aortas. In eNOS-Tg aortas, eNOS dimer:monomer was significantly depleted compared with wild type ($P<0.05$) but unchanged in GCH-Tg mice (Figure 1B). Importantly, the reduced eNOS dimer:monomer ratio in the eNOS-Tg group was restored to wild-type levels in double- transgenic eNOS/GCH-Tg mice.

We investigated the subcellular localization of eNOS in primary cultures of lung endothelial cells using immunocytochemistry. eNOS appeared to be localized mainly to plasma

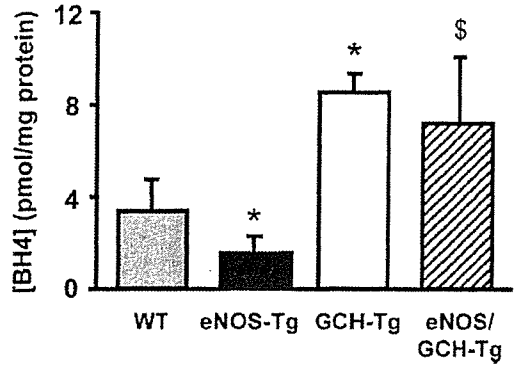

Figure 2. BH4 levels in aortas from wild-type (WT), eNOS-Tg, GCH-Tg, and eNOS/GCH-Tg mice. *$P<0.05$ compared with WT and \$$P<0.05$ compared with eNOS-Tg; n=6 to 8 animals per group.

membranes and the Golgi apparatus in endothelial cells from all 4 groups (Figure 1C). However, in accordance with the immunoblotting data, the intensity of eNOS immunostaining, unchanged in GCH-Tg mice, was markedly increased in endothelial cells from eNOS-Tg and eNOS/GCH-Tg animals compared with wild type.

Aortic BH4 Levels

We next measured vascular BH4 levels in homogenates of snap-frozen aorta using iodine oxidation and HPLC. Surprisingly, BH4 levels were significantly depleted in eNOS-Tg mice compared with wild type, suggesting oxidative degradation of BH4 ($P<0.05$; Figure 2). We then sought to confirm that increased endothelial GTPCH expression led to increased BH4 levels in aortic homogenates of GCH-Tg and eNOS/GCH-Tg mice. As reported previously,[24] aortic BH4 levels were significantly elevated by >2-fold in GCH-Tg mice compared with wild type ($P<0.05$). Importantly, aortic BH4 levels were also elevated in eNOS/GCH-Tg mice and were not significantly different between GCH-Tg and eNOS/GCH-Tg mice.

eNOS Enzymatic Activity and NO Production

To determine the relationship between eNOS protein levels and eNOS enzymatic activity, we measured conversion of ^{14}C L-arginine to ^{14}C L-citrulline by eNOS in intact aorta using HPLC with online scintillation detection. Citrulline production was increased only 2-fold in eNOS-Tg aortas compared with wild type ($P<0.05$; Figure 3A and 3B), despite eNOS protein levels being elevated 8-fold in these animals. Indeed, the ratio of eNOS enzymatic activity to eNOS protein was 0.6 in eNOS-Tg mice compared with 2.0 in wild-type animals. A similar pattern of results was obtained when using lung tissue lysates (Figure 3C). To further investigate the stoichiometric relationship between eNOS and endothelial BH4 in vivo and to determine whether increasing endothelial BH4 in eNOS-Tg mice could augment eNOS enzymatic activity, we next measured eNOS enzymatic activity in GCH-Tg and eNOS/GCH-Tg mice. NOS activity was increased 2-fold in GCH-Tg aorta and lung compared with wild type ($P<0.05$; Figure 3A through 3C). Indeed, eNOS enzymatic activity was similar in GCH-Tg and eNOS-Tg mice despite eNOS protein

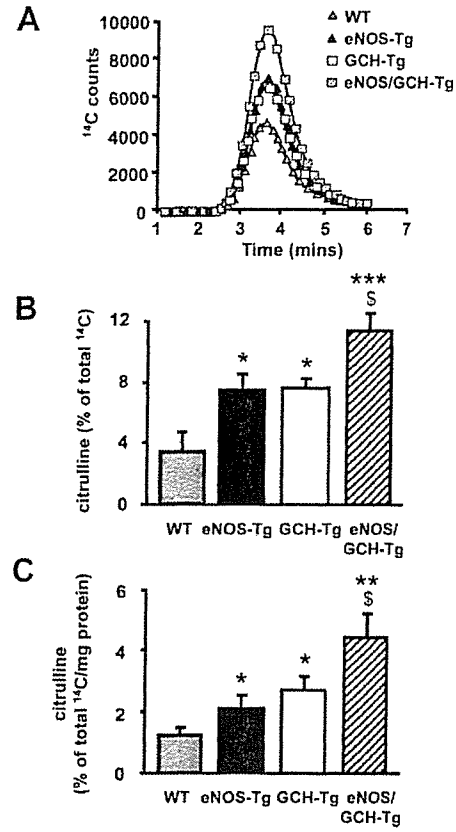

Figure 3. A, Representative HPLC chromatograms showing ^{14}C citrulline peaks for wild-type (WT; gray triangles), eNOS-Tg (black triangles), GCH-Tg (white squares), and eNOS/GCH-Tg (hatched squares) mouse aortas. Graphs show percentage ^{14}C citrulline conversion from ^{14}C arginine as a measure of eNOS activity measured in total fresh intact aorta (B) and lung tissue lysates (C); n=5 to 8 animals per group; *$P<0.05$, **$P<0.01$, and ***$P<0.001$ compared with WT; and \$$P<0.05$ compared with eNOS-Tg.

levels being considerably higher in eNOS-Tg animals. Critically, eNOS enzymatic activity was further elevated in eNOS/GCH-Tg mice compared with eNOS-Tg animals ($P<0.05$): augmented levels of endothelial BH4 in eNOS/GCH-Tg mice resulted in an ≈4-fold increase in eNOS enzymatic activity in aorta and lung compared with wild-type mice ($P<0.01$). These data suggest that eNOS activity is exquisitely dependent on endothelial BH4 levels even in the absence of vascular disease.

In complementary experiments, we used Fe-DETC EPR to directly measure NO bioavailability in mouse aortas. In accordance with measures of enzymatic activity, net NO levels were increased ≈2-fold in eNOS-Tg aortas compared with wild type (Figure 4). These results demonstrate that there was a striking discordance between eNOS protein levels, eNOS enzymatic activity, and NO production in eNOS-Tg mice. We then determined the effects of increased endothelial BH4 using the GCH-Tg and eNOS/GCH-Tg mice and observed a similar pattern of results as for NOS enzymatic activity. Aortic NO bioavailability was elevated almost 2-fold in GCH-Tg mice compared with wild type and not significantly different from eNOS-Tg mice (Figure 4). Criti-

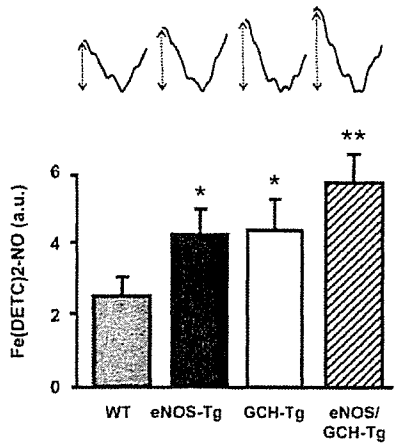

Figure 4. Net NO levels in intact aorta measured using Fe-DETC EPR. Graph shows mean quantitative data with corresponding representative EPR spectra showing the characteristic peaks associated with the Fe-DETC signal above. n=8 to 11 animals per group; *$P<0.05$ and **$P<0.01$ compared with wild type (WT). a.u. indicates arbitrary units.

cally, net NO bioavailability was further elevated (≈3-fold compared with wild type) in eNOS/GCH-Tg mice.

eNOS Uncoupling: Effect of eNOS and GTPCH Overexpression In Vivo

To investigate whether eNOS uncoupling results from discordance between eNOS and BH4, we measured $O_2^{\cdot-}$ production and, more specifically, eNOS-derived $O_2^{\cdot-}$ production using the NOS inhibitor L-NAME. We first measured $O_2^{\cdot-}$ production in tissue lysates using lucigenin chemiluminescence. Chemiluminescence was increased 2-fold in eNOS-Tg mice compared with wild-type animals ($P<0.05$; Figure 5A) but was unchanged in GCH-Tg mice. Critically, $O_2^{\cdot-}$ production was restored in eNOS/GCH-Tg mice. The proportion of $O_2^{\cdot-}$ production attributable to uncoupled NOS, assessed by quantifying L-NAME–inhibitable chemiluminescence, was significantly increased in eNOS-Tg lysates compared with wild type, indicating increased NOS uncoupling ($P<0.05$; Figure 5B). L-NAME–inhibitable chemiluminescence was unchanged in GCH-Tg mice. The presence of the GTPCH transgene in eNOS/GCH-Tg mice restored the enhanced L-NAME–inhibitable chemiluminescence of the eNOS-Tg group back to wild-type levels. We also investigated $O_2^{\cdot-}$ production in intact aorta under basal conditions and after incubation with L-NAME using lucigenin chemiluminescence and saw a similar pattern of results. Basal chemiluminescence was significantly increased in eNOS-Tg aortas compared with wild type ($P<0.05$; Table). Importantly, basal $O_2^{\cdot-}$ production in GCH-Tg and eNOS/GCH-Tg aortas was similar to wild type. Incubation of aortas with L-NAME caused a significant reduction in the $O_2^{\cdot-}$ signal in eNOS-Tg mice ($P<0.05$), indicating NOS uncoupling. However, L-NAME had little effect in wild-type, GCH-Tg, and eNOS/GCH-Tg aortas, suggesting that NOS coupling is preserved in these mice. Together, these observations suggest that in eNOS-Tg mice elevated $O_2^{\cdot-}$ production is at least partly attributable to uncoupled NOS, likely resulting from discordance between eNOS protein and endothelial BH4 because NOS coupling is preserved by increasing endothelial BH4 in association with elevated eNOS levels in eNOS/GCH-Tg animals.

Lucigenin Chemiluminescence to Measure $O_2^{\cdot-}$ Production in Intact Aortas Incubated for 30 Minutes at 37°C in the Presence or Absence of L-NAME (1 mmol/L)

	Wild Type	eNOS-Tg	GCH-Tg	eNOS/GCH-Tg
Basal, RLU/s/mg	39.5±4.5	59.7±6.6*	52.8±5.8	46.2±4.7
+ L-NAME, RLU/s/mg	42.5±10.1	39.2±4.8†	54.0±13.2	49.3±11.2

Results are expressed as counts per second per milligram of dry weight of aorta.

*$P<0.05$compared with wild type; †$P<0.05$ compared with baseline (without L-NAME).

RLU indicates relative light units.

To investigate $O_2^{\cdot-}$ production specifically from the aortic endothelium, we quantified endothelial DHE fluorescence using oxidative confocal microtopography. Endothelial DHE fluorescence was increased 2-fold in eNOS-Tg mice compared with wild-type and GCH-Tg mice (Figure 6). Impor-

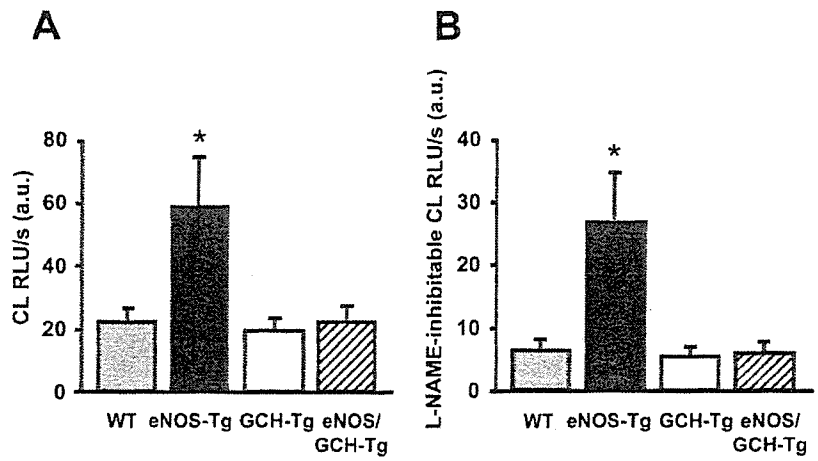

Figure 5. Lucigenin (5μmol/L) chemiluminescence (CL) in cardiac tissue lysates from wild-type (WT), eNOS-Tg, GCH-Tg, and eNOS/GCH-Tg mice to measure basal $O_2^{\cdot-}$ production (A) and L-NAME (1 mmol/L)–inhibitable $O_2^{\cdot-}$ production (B) as a marker of NOS uncoupling. *$P<0.05$ compared with WT; n=7 to 10 animals per group. RLU indicates relative light units; a.u., arbitrary units.

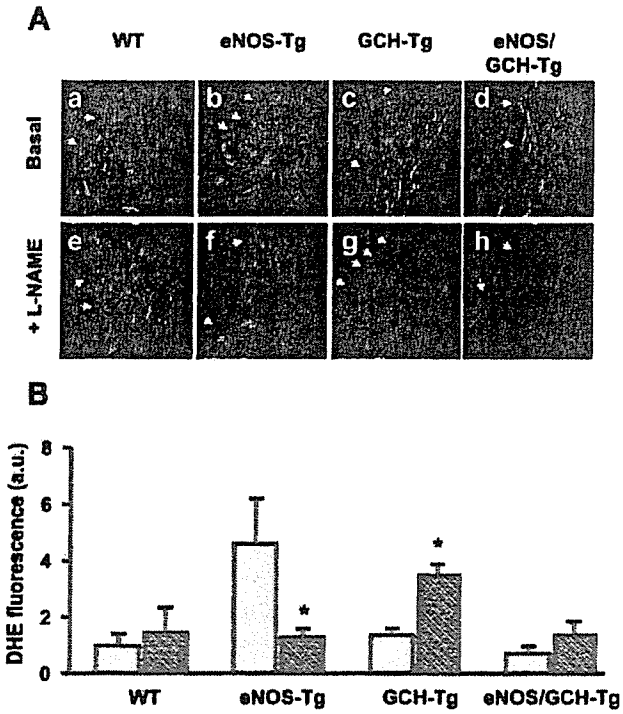

Figure 6. DHE staining, to measure in situ $O_2^{\cdot-}$ production, in aortic sections. A, Representative aortic sections (×60) showing red endothelial cells (arrows) from wild-type (WT; a and e), eNOS-Tg (b and f), GCH-Tg (c and g), and eNOS/GCH-Tg (d and h) mice in the presence (e through h) and absence (a through d) of L-NAME (1 mmol/L). B, Quantified specific endothelial DHE fluorescence is expressed for sections in the presence (hatched bars) and absence (gray bars) of L-NAME in arbitrary units (a.u.) for each group. *$P<0.05$ comparing sections in the presence or absence of L-NAME; n=5 to 7 animals per group.

tantly, endothelial fluorescence was restored to wild-type levels in eNOS/GCH-Tg mice. Fluorescence from the other layers of the vessel wall was not significantly different between groups. Incubation with L-NAME had little effect in wild-type aortas but reversed the elevated DHE signal in eNOS-Tg endothelium back to wild-type levels, again indicating that the source of $O_2^{\cdot-}$ was likely uncoupled eNOS. In contrast, L-NAME significantly increased the endothelial $O_2^{\cdot-}$ signal in GCH-Tg mice, indicating that in these aortas, eNOS was predominantly coupled and producing NO. Critically, as in wild-type aortas, NOS inhibition with L-NAME had little effect in eNOS/GCH-Tg mice, indicating restored eNOS coupling compared with eNOS-Tg animals. In accordance with the data for $O_2^{\cdot-}$ production measured by chemiluminescence, these results suggest that increased eNOS uncoupling in eNOS-Tg aortas increases eNOS-derived $O_2^{\cdot-}$, but that eNOS coupling is, at least in part, preserved by increased endothelial BH4 synthesis in eNOS/GCH-Tg mice.

Discussion

In this study, we describe a new double-transgenic mouse model in which endothelial-targeted overexpression of GTPCH leads to increased endothelial BH4 levels in mice with endothelial-targeted eNOS overexpression. We used this model to investigate the role of BH4 in the regulation of eNOS coupling in vivo, specifically in the absence of pathological oxidative stress associated with vascular disease states.[6] The major findings in this study are as follows. First, eNOS protein levels are markedly elevated in eNOS-Tg and eNOS/GCH-Tg mice but not in GCH-Tg animals, although the proportion of eNOS dimer to monomer is depleted only in eNOS-Tg aortas. Second, endothelial-specific overexpression of GTPCH is sufficient to increase vascular BH4 levels in GCH-Tg and in eNOS/GCH-Tg aortas, whereas BH4 levels are depleted in eNOS-Tg aortas. Third, this increase in BH4 is sufficient to augment vascular eNOS enzymatic activity even in GCH-Tg mice, which have unchanged eNOS protein levels. Indeed, eNOS activity is similar between GCH-Tg and eNOS-Tg mice despite eNOS-Tg mice having 8-fold more eNOS protein. Importantly, the increase in endothelial BH4 in eNOS/GCH-Tg mice further enhances eNOS activity and NO bioavailability compared with eNOS-Tg mice. Fourth, the discordance between endothelial BH4 and eNOS protein in eNOS-Tg mice results in uncoupled eNOS and increased NOS-derived $O_2^{\cdot-}$ production in tissue lysates and intact aorta. However, increased vascular BH4 in eNOS/GCH-Tg mice is sufficient, at least in part, to restore eNOS coupling, increase NO production, and reduce eNOS-dependent $O_2^{\cdot-}$ production.

These findings provide important insights into the role of endothelial BH4 synthesis in regulating eNOS activity and eNOS coupling even in the absence of vascular oxidative stress. Previous studies have reported that endothelial dysfunction in vascular diseases, such as hypertension,[12] diabetes,[24] and atherosclerosis,[26] is associated with increased $O_2^{\cdot-}$ production deriving principally from NADPH oxidases.[7,8] Landmesser et al[12] demonstrated that the increase in NADPH oxidase–derived $O_2^{\cdot-}$ in deoxycorticosterone acetate–salt hypertensive mice led to enhanced oxidation of BH4, resulting in eNOS uncoupling, increased eNOS-derived $O_2^{\cdot-}$ production, and reduced NO formation, thereby exacerbating oxidative stress. Oral supplementation with BH4, or a reduction in NADPH oxidase activity (using p47phox−/− mice), reversed eNOS uncoupling. However, the mechanistic relationship between eNOS and its cofactor BH4 has not been investigated in vivo in the absence of pathological oxidative stress. We now show that a stoichiometric discordance between eNOS protein and BH4 levels is alone sufficient to cause eNOS uncoupling, and that eNOS uncoupling in the absence of vascular disease is sufficient to deplete BH4 levels by oxidation. Laursen et al[19] demonstrated that peroxynitrite may be the principal ROS involved in oxidation of BH4.

NO, constitutively produced by eNOS in the vascular endothelium, is a potent vasodilator and exerts numerous vasoprotective antiatherogenic effects. Reduced NO bioactivity is an early feature of a number of vascular diseases, including atherosclerosis.[5] Short-term in vivo gene transfer of eNOS or neuronal NOS can improve NO-mediated vascular relaxation in atherosclerotic arteries.[34] However, previous studies investigating the possible vasoprotective effects of chronic eNOS overexpression in eNOS-Tg mice have yielded conflicting results. Kawashima et al[35] demonstrated reduced lesion formation after carotid artery ligation in eNOS-Tg mice. In contrast, Ozaki et al,[10] using the same strain of

eNOS-Tg mice as used in the present study, found that eNOS overexpression accelerated rather than reduced atherosclerosis in apolipoprotein E knockout mice, at least in part, because of eNOS uncoupling and $O_2^{\cdot-}$ generation. In the present study, using a mouse model not exposed to pathological vascular oxidative stress, we also show that eNOS-derived $O_2^{\cdot-}$ production is enhanced in eNOS-Tg mice, in cardiac tissue lysates and intact aorta, indicating increased eNOS uncoupling in these animals. We performed additional experiments, using quantitative RT-PCR, to confirm that the increased $O_2^{\cdot-}$ in eNOS-Tg animals is not a result of a concomitant increase in the expression of the NADPH oxidase system, a major source of vascular $O_2^{\cdot-}$ generation (data not shown). These findings agree with those from Ohashi et al[25] using nondiseased eNOS-Tg mice. This enhanced vascular oxidative stress may account for the depleted aortic BH4 levels observed in the eNOS-Tg mice because BH4 is readily oxidized by ROS to BH2 that is inactive for eNOS cofactor function. In accordance with having increased uncoupled eNOS and depleted BH4 levels, specific NOS enzymatic activity is markedly attenuated in eNOS-Tg mice (elevated only 2-fold compared with wild type) relative to eNOS protein levels (elevated 8-fold compared with wild type). Indeed, the ratio of eNOS enzymatic activity to eNOS protein was only 0.6 in eNOS-Tg mice compared with 2.0 in wild-type animals.

Several previous studies have established that BH4 is a required cofactor for NOS activity.[9,28,36] Recent studies, including those in atherosclerotic eNOS-Tg mice,[10] have demonstrated that NOS uncoupling can be reversed and NOS enzymatic activity increased by augmenting BH4 levels.[10,12] However, an advantage of the present study is that by targeting overexpression of GTPCH, the rate-limiting enzyme in BH4 biosynthesis, to the vascular endothelium, we avoid the potential confounding antioxidant effects of high-dose pharmacological BH4 supplementation used in other studies.[10,12] Furthermore, we have been able to specifically evaluate the role of endothelial BH4, as opposed to systemic BH4, in the regulation of eNOS activity. Importantly, using 2 methods to measure $O_2^{\cdot-}$ production in cardiac tissue and intact aorta, as well as specifically in aortic endothelium, we demonstrate that NOS-dependent $O_2^{\cdot-}$ generation, elevated in eNOS-Tg mice, is normalized in eNOS/GCH-Tg mice. These data support the hypothesis that discordance between eNOS protein and endothelial BH4 levels is sufficient to cause eNOS uncoupling even in the absence of pathological oxidative stress. In support of this conclusion, NOS enzymatic activity and the ratio of enzymatic activity relative to eNOS protein levels were increased in eNOS/GCH-Tg compared with eNOS-Tg mice. Interestingly, GCH-Tg mice also had increased NOS enzymatic activity compared with wild type, indicating that even in the absence of either enhanced eNOS protein or disease, BH4 levels may limit eNOS enzymatic activity in vivo. These data therefore suggest that eNOS activity (to generate NO) can be augmented by modestly increasing BH4 levels, specifically in the endothelium, even under normal physiological conditions.

Previous data have shown that eNOS dimerization is an important aspect of eNOS activation and NO production.[28] BH4 has been suggested to increase the stability of the eNOS homodimer such that the ratio of dimer to monomer is increased.[28,37] In eNOS-Tg mice, the discordance between high levels of eNOS protein and depleted aortic BH4 levels may account for the relative decrease in homodimeric eNOS protein that we observed. In support, the increased production of endothelial BH4 in eNOS/GCH-Tg mice was sufficient to maintain the ratio of eNOS dimer to monomer. These in vivo findings corroborate previous in vitro studies suggesting that an important action of BH4, in addition to its direct contribution to electron transport within the eNOS active site, is to maintain eNOS in its homodimeric conformation.

We conclude that eNOS uncoupling is an independent and direct consequence of a stoichiometric discordance between enzyme and its cofactor BH4. BH4 is critical for regulating eNOS activity and its production of NO, as opposed to $O_2^{\cdot-}$, even in the absence of increased oxidative stress associated with vascular disease states. Thus, strategies to increase eNOS protein without a concomitant augmentation of endothelial BH4 levels may lead to eNOS uncoupling and paradoxically exacerbate oxidative stress and the progression of vascular diseases. Although reduced biosynthesis of BH4 may not be the principal mechanism of BH4 loss in vascular disease, strategies aimed at increasing BH4 synthesis or reducing BH4 oxidation may be valid therapeutic approaches in vascular disease states.

Acknowledgments

This work was supported by the British Heart Foundation (RG02/007) and the Wellcome Trust.

References

1. Ignarro LJ. Nitric oxide as a unique signaling molecule in the vascular system: a historical overview. *J Physiol Pharmacol.* 2002;53:503–514.
2. Furchgott RF, Zawadzki JV. The obligatory role of endothelial cells in the relaxation of arterial smooth muscle by acetylcholine. *Nature.* 1980;288:373–376.
3. Panza JA, García CE, Kilcoyne CM, Quyyumi AA, Cannon RO III. Impaired endothelium-dependent vasodilation in patients with essential hypertension: evidence that nitric oxide abnormality is not localized to a single signal transduction pathway. *Circulation.* 1995;91:1732–1738.
4. Schachinger V, Britten MB, Zeiher AM. Prognostic impact of coronary vasodilator dysfunction on adverse long-term outcome of coronary heart disease. *Circulation.* 2000;101:1899–1906.
5. Heitzer T, Schlinzig T, Krohn K, Meinertz T, Munzel T. Endothelial dysfunction, oxidative stress, and risk of cardiovascular events in patients with coronary artery disease. *Circulation.* 2001;104:2673–2678.
6. Cai H, Harrison DG. Endothelial dysfunction in cardiovascular diseases: the role of oxidant stress. *Circ Res.* 2000;87:840–844.
7. Griendling KK, Sorescu D, Ushio-Fukai M. NAD(P)H oxidase: role in cardiovascular biology and disease. *Circ Res.* 2000;86:494–501.
8. Guzik TJ, West NEJ, Black E, McDonald D, Ratnatunga C, Pillai R, Channon KM. Vascular superoxide production by NAD(P)H oxidase: association with endothelial dysfunction and clinical risk factors. *Circ Res.* 2000;86:e85–e90.
9. Vasquez-Vivar J, Kalyanaraman B, Martasek P, Hogg N, Masters BS, Karoui H, Tordo P, Pritchard KA Jr. Superoxide generation by endothelial nitric oxide synthase: the influence of cofactors. *Proc Natl Acad Sci U S A.* 1998;95:9220–9225.
10. Ozaki M, Kawashima S, Yamashita T, Hirase T, Namiki M, Inoue N, Hirata K-i, Yasui H, Sakurai H, Yoshida Y, Masada M, Yokoyama M. Overexpression of endothelial nitric oxide synthase accelerates atherosclerotic lesion formation in apoE-deficient mice. *J Clin Invest.* 2002;110:331–340.
11. Vasquez-Vivar J, Kalyanaraman B, Martasek P. The role of tetrahydrobiopterin in superoxide generation from eNOS: enzymology and physiological implications. *Free Radic Res.* 2003;37:121–127.

12. Landmesser U, Dikalov S, Price SR, McCann L, Fukai T, Holland SM, Mitch WE, Harrison DG. Oxidation of tetrahydrobiopterin leads to uncoupling of endothelial cell nitric oxide synthase in hypertension. *J Clin Invest.* 2003;111:1201–1209.
13. Maier W, Cosentino F, Lutolf RB, Fleisch M, Seiler C, Hess OM, Meier B, Luscher TF. Tetrahydrobiopterin improves endothelial function in patients with coronary artery disease. *J Cardiovasc Pharmacol.* 2000;35: 173–178.
14. Guzik TJ, Mussa S, Gastaldi D, Sadowski J, Ratnatunga C, Pillai R, Channon KM. Mechanisms of increased vascular superoxide production in human diabetes mellitus: role of NAD(P)H oxidase and endothelial nitric oxide synthase. *Circulation.* 2002;105:1656–1662.
15. Heitzer T, Yla-Herttuala S, Luoma J, Kurz S, Munzel T, Just H, Olschewski M, Drexler H. Cigarette smoking potentiates endothelial dysfunction of forearm resistance vessels in patients with hypercholesterolemia. Role of oxidized LDL. *Circulation.* 1996;93:1346–1353.
16. Alp NJ, Channon KM. Regulation of endothelial nitric oxide synthase by tetrahydrobiopterin in vascular disease. *Arterioscler Thromb Vasc Biol.* 2004;24:413–420.
17. Vasquez-Vivar J, Whitsett J, Martasek P, Hogg N, Kalyanaraman B. Reaction of tetrahydrobiopterin with superoxide: EPR-kinetic analysis and characterization of the pteridine radical. *Free Radic Biol Med.* 2001; 31:975–985.
18. Zheng J-S, Yang X-Q, Lookingland KJ, Fink GD, Hesslinger C, Kapatos G, Kovesdi I, Chen AF. Gene transfer of human guanosine 5'-triphosphate cyclohydrolase I restores vascular tetrahydrobiopterin level and endothelial function in low renin hypertension. *Circulation.* 2003;108:1238–1245.
19. Laursen JB, Somers M, Kurz S, McCann L, Warnholtz A, Freeman BA, Tarpey M, Fukai T, Harrison DG. Endothelial regulation of vasomotion in apoE-deficient mice: implications for interactions between peroxynitrite and tetrahydrobiopterin. *Circulation.* 2001;103:1282–1288.
20. Kuzkaya N, Weissmann N, Harrison DG, Dikalov S. Interactions of peroxynitrite, tetrahydrobiopterin, ascorbic acid, and thiols: implications for uncoupling endothelial nitric-oxide synthase. *J Biol Chem.* 2003;278: 22546–22554.
21. Vasquez-Vivar J, Martasek P, Whitsett J, Joseph J, Kalyanaraman B. The ratio between tetrahydrobiopterin and oxidized tetrahydrobiopterin analogues controls superoxide release from endothelial nitric oxide synthase: an EPR spin trapping study. *Biochem J.* 2002;362:733–739.
22. Vasquez-Vivar J, Martasek P, Kalyanaraman B. Superoxide generation from nitric oxide synthase: role of cofactors and protein interaction. In: *Biological Magnetic Resonance.* Boston, Mass: Kluwer Academic Publishers; 2005:75–91.
23. Rodriguez-Crespo I, Gerber NC, Ortiz de Montellano PR. Endothelial nitric-oxide synthase. Expression in *Escherichia coli*, spectroscopic characterization, and role of tetrahydrobiopterin in dimer formation. *J Biol Chem.* 1996;271:11462–11467.
24. Alp NJ, Mussa S, Khoo J, Guzik TJ, Cai S, Jefferson A, Rockett KA, Channon KM. Tetrahydrobiopterin-dependent preservation of nitric oxide-mediated endothelial function in diabetes by targeted transgenic GTP-cyclohydrolase I overexpression. *J Clin Invest.* 2003;112:725–735.
25. Ohashi Y, Kawashima S, Hirata K, Yamashita T, Ishida T, Inoue N, Sakoda T, Kurihara H, Yazaki Y, Yokoyama M. Hypotension and reduced nitric oxide-elicited vasorelaxation in transgenic mice overexpressing endothelial nitric oxide synthase. *J Clin Invest.* 1998;102: 2061–2071.
26. Alp NJ, McAteer MA, Khoo J, Choudhury RP, Channon KM. Increased endothelial tetrahydrobiopterin synthesis by targeted transgenic GTP-cyclohydrolase I overexpression reduces endothelial dysfunction and atherosclerosis in ApoE-knockout mice. *Arterioscler Thromb Vasc Biol.* 2004;24:445–450.
27. Klatt P, Schmidt K, Lehner D, Glatter O, Bachinger HP, Mayer B. Structural analysis of porcine brain nitric oxide synthase reveals a role for tetrahydrobiopterin and L-arginine in the formation of an SDS- resistant dimer. *EMBO J.* 1995;14:3687–3695.
28. Cai S, Alp NJ, Mc Donald D, Canevari L, Heales S, Channon KM. GTP cyclohydrolase I gene transfer augments intracellular tetrahydrobiopterin in human endothelial cells: effects on nitric oxide synthase activity, protein levels and dimerization. *Cardiovasc Res.* 2002;55:838–849.
29. Rockett KA, Brookes R, Udalova I, Vidal V, Hill AV, Kwiatkowski D. 1,25-Dihydroxyvitamin D3 induces nitric oxide synthase and suppresses growth of Mycobacterium tuberculosis in a human macrophage-like cell line. *Infect Immun.* 1998;66:5314–5321.
30. Kleschyov AL, Munzel T. Advanced spin trapping of vascular nitric oxide using colloid iron diethyldithiocarbamate. *Methods Enzymol.* 2002; 359:42–51.
31. Bendall JK, Heymes C, Wright TJ, Wheatcroft S, Grieve DJ, Shah AM, Cave AC. Strain-dependent variation in vascular responses to nitric oxide in the isolated murine heart. *J Mol Cell Cardiol.* 2002;34:1325–1333.
32. Skatchkov MP, Sperling D, Hink U, Mulsch A, Harrison DG, Sindermann I, Meinertz T, Munzel T. Validation of lucigenin as a chemiluminescent probe to monitor vascular superoxide as well as basal vascular nitric oxide production. *Biochem Biophys Res Commun.* 1999;254:319–324.
33. Khan SA, Lee K, Minhas KM, Gonzalez DR, Raju SVY, Tejani AD, Li D, Berkowitz DE, Hare JM. Neuronal nitric oxide synthase negatively regulates xanthine oxidoreductase inhibition of cardiac excitation-contraction coupling. *Proc Natl Acad Sci U S A.* 2004;101:15944–15948.
34. Channon KM, Qian HS, Neplioueva V, Blazing MA, Olmez E, Shetty GA, Youngblood SA, Stamler JS, George SE. In vivo gene transfer of nitric oxide synthase enhances vasomotor function in carotid arteries from normal and cholesterol-fed rabbits. *Circulation.* 1998;98:1905–1911.
35. Kawashima S, Yamashita T, Ozaki M, Ohashi Y, Azumi H, Inoue N, Hirata K-i, Hayashi Y, Itoh H, Yokoyama M. Endothelial NO synthase overexpression inhibits lesion formation in mouse model of vascular remodeling. *Arterioscler Thromb Vasc Biol.* 2001;21:201–207.
36. Tzeng E, Billiar TR, Robbins PD, Loftus M, Stuehr DJ. Expression of human inducible nitric oxide synthase in a tetrahydrobiopterin (H4B)-deficient cell line—H4B promotes assembly of enzyme subunits into an active enzyme. *Proc Natl Acad Sci U S A.* 1995;92:11771–11775.
37. Wever RMF, van Dam T, van Rijn HJ, de Groot F, Rabelink TJ. Tetrahydrobiopterin regulates superoxide and nitric oxide generation by recombinant endothelial nitric oxide synthase. *Biochem Biophys Res Commun.* 1997;237:340–344.

A Randomized Clinical Study of Tea Catechin Inhalation Effects on Methicillin-Resistant *Staphylococcus aureus* in Disabled Elderly Patients

Hiroshi Yamada, MD, Masato Tateishi, MD, Kazuhiro Harada, MD, Toshihiko Ohashi, MD, Takako Shimizu, MD, Tetsushi Atsumi, MD, Yasuko Komagata, PhD, Hajime Iijima, PhD, Kanki Komiyama, PhD, Hiroshi Watanabe, MD, Yukihiko Hara, PhD, and Kyoichi Ohashi, MD

Objectives: To evaluate the effects of tea catechin inhalation on methicillin-resistant *Staphylococcus aureus* (MRSA) in disabled elderly patients.

Design: Seven days, randomized, prospective study.

Setting: Three hospitals in Japan.

Participants: Seventy-two patients aged 78 ± 11 years (mean age ± standard deviation) with cerebrovascular diseases, classified as disabled according to the activity of daily living and were either bedridden or required assistance for standing, and showing presence of MRSA in sputum.

Interventions: Inhalation of 2 mL tea catechin extract solution along with saline (3.7 mg/mL catechins, 43% of catechins are composed of epigallocatechin gallate), or saline alone, 3 times daily using a handheld nebulizer for 7 days.

Measurements: The endpoint of efficacy was the reduction rates of MRSA in sputum. The safety measure was the adverse events observed during the 7 days of inhalation.

Results: The reduction rates calculated as the summation of decrease and disappearance of MRSA in sputum at 7 days were 47% (17 of 36 patients) in the catechin group and 15% (5 of 33 patients) in the control group; the difference in the reduction rates between the 2 groups was statistically significant ($P = .014$). The disappearance rate of MRSA in sputum was higher in the catechin group (31%; 11 patients) when compared with the control group (12%; 4 patients), however the difference in the disappearance rate between the 2 groups was not statistically significant ($P = .091$). No adverse events, such as respiratory tract obstruction, allergic bronchial spasm, or skin eruption, including laboratory changes, were observed during the study.

Conclusion: The catechin inhalation appeared to reduce the MRSA count in sputum. However, the application of tea catechin inhalation as a supplementary treatment for controlling MRSA infection remains controversial. **(J Am Med Dir Assoc 2006; 7: 79–83)**

Keywords: Methicillin-resistant Staphylococcus aureus *(MRSA); catechin; elderly; disabled*

Methicillin-resistant *Staphylococcus aureus* (MRSA) is a multidrug-resistant pathogen and is often responsible for serious nosocomial infections associated with significant mortality and morbidity. MRSA often causes life-threatening infections, such as pneumonia or sepsis, in some susceptible patients using immunosuppressant drugs or in the disabled elderly.[1,2] Patients who are colonized or infected with MRSA can cause serious social implications such as hospital-acquired infections or prolonged hospitalization. Moreover, patients with MRSA, particularly elderly patients, are usually isolated, depressed, and suffer from anxiety, which in turn decreases their quality of life.[3] Therefore, control of MRSA is essential for social benefits as well as for the improvement in the health and quality of life of the elderly patients.

Catechins are the major components of tea flavonoids and

Division of Drug Evaluation and Informatics, University of Shizuoka, Shizuoka, Japan (H.Y.); Department of Hospital Pharmacy, National Hospital Organization, Fukuoka Higashi Medical Center, Koga, Japan (M.T.); Department of Internal Medicine, Kasaoka Daiichi Hospital, Kasaoka, Japan (K.H.); Department of Neurology, Seirei Hamamatsu General Hospital, Hamamatsu, Japan (T.O., T.S., T.A.); Research Center for Clinical Pharmacology, The Kitasato Institute, Tokyo, Japan (Y.K., H.I., K.K.); Mitsui Norin Co. Ltd., Tokyo, Japan (Y.H.); Department of Clinical Pharmacology and Therapeutics, Hamamatsu University School of Medicine, Hamamatsu, Japan (H.W., K.O.).

Address correspondence to Hiroshi Yamada, MD, PhD, FACP, Division of Drug Evaluation and Informatics, School of Pharmaceutical Sciences, University of Shizuoka, 52-1 Yada, Suruga-ku, Shizuoka, 422-8526 Japan. E-mail: hyamada@u-shizuoka-ken.ac.jp

DOI: 10.1016/j.jamda.2005.06.002

are reported to possess antioxidative, anticancer, hypolipidemic, hypoglycemic, hypotensive, antiviral, and antibacterial effects.[4–6] Recent in vitro experimental studies have revealed that tea catechin extracts induce bactericidal effects as well as demonstrate synergistic effects with antibiotics against MRSA.[7–15] However, thus far, a limited number of studies have been conducted on the clinical effects of tea catechin against MRSA.[16–18] In our previous clinical pilot studies, catechin inhalation showed a temporary effect on the elimination of MRSA in sputum, and this effect was observed in a dose-dependent manner.[17,18] Based on these results, we designed a prospective randomized controlled study to evaluate the effects of tea catechin inhalation on MRSA in disabled elderly patients.

METHODS

A total of 72 inpatients who attended the Department of Neurology at Seirei Hamamatsu General Hospital, Department of Internal Medicine at National Hospital Organization Fukuoka Higashi Medical Center, and Kasaoka Daiichi Hospital, and showed presence of MRSA in their sputum samples were studied between February 2002 and April 2004. The mean age of all patients was 78 ± 11 years, and the patients were randomized prior to receiving inhalation treatment. All study patients had a history of cerebrovascular diseases and were classified as disabled according to the activity of daily living; these patients were either bedridden or required assistance for standing. Cerebrovascular diseases in the patients were diagnosed using magnetic resonance imaging or computerized tomography of the brain. The study was approved by the ethics committee at each study site and was conducted in accordance with the Declaration of Helsinki. Written informed consent was obtained from all patients or their guardians before participation in the study.

The patients were recruited sequentially and were randomized in a single-blind manner. Randomized allocation was performed independently at the Hamamatsu University School of Medicine, and the requisite information was provided to investigative staff at each site. The study patients and guardians were not informed of the type of material in the nebulizer. To estimate the effectiveness of tea catechin inhalation on patients' clinical outcomes, sputum samples were tested at each site by a laboratory technician who had no prior information regarding which of the patients were allocated to the control group or to the catechin group. The patients included in the catechin group received inhalation of 2 mL tea catechin extract solution in saline, and the control group received inhalation of saline alone. The concentration of the catechin solution in saline was equivalent to 3.7 mg/mL catechins; these catechins were composed of 1.6 mg epigallocatechin gallate (EGCG). Using a handheld nebulizer, the catechin solution was inhaled 3 times daily for a period of 7 days. Catechins were in the form of polyphenon 60A (Mitsui Norin Co, Ltd, Tokyo, Japan), and total catechin content was 73.0%, including 31% (−)-EGCG, 21% (−)-epigallocatechin, 8.6% (−)-epicatechin, 8.6% (−)-epicatechin gallate, 2.9% (−)-gallocatechin gallate, and 0.8% (−)-catechin gallate.

Staphylococcus aureus isolated from the sputum was defined as MRSA when it showed a minimum inhibitory concentration (MIC) of more than 4 μg/mL for oxacillin in a disk diffusion method of the National Committee for Clinical Laboratory Standards (NCCLS). All the strains were identified by polymerase chain reaction (PCR) analysis of *mecA* gene expression.[19] If the patients faced difficulties in expectorating sputum themselves, they were assisted by registered nurses. The microbiology laboratory at each hospital evaluated the quality of sputum. The samples of sputum that showed resistance to oxacillin in the disk diffusion test were evaluated for MRSA colony formation units (CFU) using routine laboratory tests; the count of MRSA as CFU was graded based on a semiquantitive scale of 0, 1+, 2+, or 3+. The enrolled patients were confirmed to show an MRSA count of 2+ or 3+ on the CFU scale in their sputum samples at least twice a week prior to their allocation. If a patient was observed to have an MRSA infection, the antibiotic therapy was continued and was not changed during the study. Infected patients were defined as those who exhibited the clinical symptoms of infection, such as bronchopneumonia, along with the presence of MRSA in their sputum samples. On the other hand, colonized patients were defined as those who did not exhibit clinical symptoms of infection, but showed presence of MRSA in their sputum samples. Patients were excluded from participation in the study if they had a history of bronchial asthma; hypersensitivity to tea ingestion; or severe cardiac, renal, or hepatic dysfunction.

For the estimation of patients' clinical outcomes, the reduction rates calculated as the summation of decrease and disappearance of MRSA in sputum between the 2 groups were compared at the beginning and at the end of the inhalation. A decrease in MRSA count was defined as a 2-scale improvement from 3+ to 1+, and the disappearance of MRSA was defined as the change in the count to scale 0. MRSA in sputum was confirmed twice at the end of inhalation, and the higher score was selected for analysis. For the safety evaluations, laboratory data were measured before and after 1 week of inhalation, and the adverse events such as respiratory tract obstruction, allergic bronchial spasm, or skin eruption were also checked at each inhalation time during the study.

All statistical analyses were performed using SPSS for Windows, version 11.0 (SPSS, Inc, Chicago, IL). Data of continuous variables are expressed as means ± SD. The differences in the quantitative data between the groups were assessed by the Student *t* test. The chi-square test was used to compare categorical variables with variables divided in quartiles. Statistical differences in the reduction or disappearance of MRSA between the catechin group and the control group were evaluated by the multivariate logistic regression analysis. A *P* value less than .05 was considered to be statistically significant.

RESULTS

Sixty-nine patients completed the study; 3 patients dropped out because of their refusal to provide consent since they were transferred to a nursing home (Figure 1). The clinical profiles of the subjects who participated in the study are summarized in Table 1. MRSA infection was diagnosed in 16 patients, whereas 53 patients were observed to be colonized with MRSA. During the study, the infected patients were administered a glycopep-

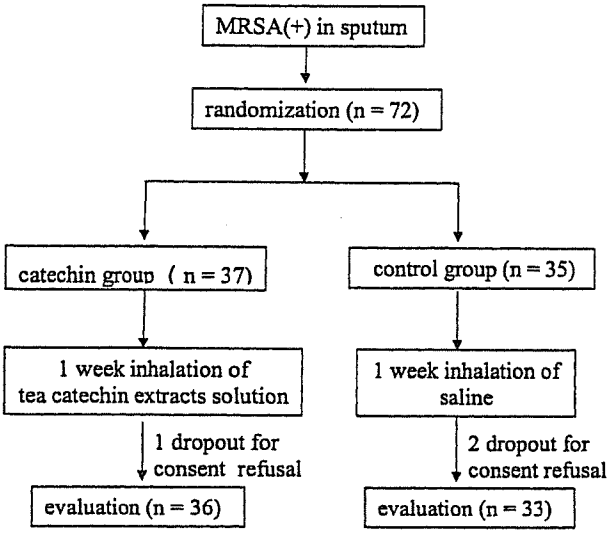

Fig. 1. *Flow of the study protocol.*

tide or aminoglycoside antibiotic, such as vancomycin, teicoplanin, or arbekacin, in combination with other antibiotics. On the other hand, no antibiotics were administered to the colonized patients. Forty-one patients were catheterized with a nasogastric, tracheal, or urethral tube. No significant differences were observed between the catechin group and the control group with respect to age, sex, MRSA infection or colonization status, degree of activity of daily living, existence of decubitus ulcers, catheterization, and laboratory data for indications of anemia, nutritional status, inflammation, or hepatic or renal dysfunction.

After 1 week of inhalation, the reduction rates calculated as the summations of decrease and disappearance of MRSA in sputum were 47% (17 of 36 patients) in the catechin group and 15% (5 of 33 patients) in the control group; the difference in the reduction rates between the 2 groups was observed to be statistically significant (P = .014). The disappearance rate of MRSA in sputum was higher in the catechin group (31%; 11 patients) when compared with that in the control group (12%; 4 patients); however, the difference in the disappearance rate between the 2 groups was not statistically significant (P = .091) (Table 2).

In the subgroup analysis of 53 patients colonized with MRSA, the reduction rates of MRSA were 50% (13 of 26 patients) in the catechin group and 19% (5 of 27 patients) in the control group; the difference in the reduction rate between the 2 groups was observed to be statistically significant (P = .027). The disappearance rate of MRSA in sputum was higher in the catechin group (31%; 8 patients) when compared with that in the control group (15%; 4 patients); however, the difference in the disappearance rate between the 2 groups was not statistically significant. Of 16 patients infected with MRSA, the reduction in MRSA count was observed in 4 patients in the catechin group, whereas none of the patients in the control group showed a reduction in MRSA count. Among the 16 infected patients, 4 patients were administered vancomycin; 5, teicoplanin; and 1, arbekacin in the catechin group, whereas in the control group, 3 patients were administered vancomycin; 1, teicoplanin; and 2, arbekacin, in combination with imipenem, panipenem, or ceftazidime. Among the infected patients who showed reduction in MRSA count, one patient was administered vancomycin, whereas 3 patients were administered teicoplanin, in combina-

Table 1. *Clinical Profiles of the Catechin Inhalation Group and the Control Group*

	Catechin Group n = 36	Control Group n = 33	*P* Value
Patient age, y*	78 ± 9.5	78 ± 13	.97
Men/women	19/17	18/15	.88
MRSA infected/colonized	10/26	6/27	.89
Activity of daily living			.13
Bedridden	27	19	
Standing with assistance	9	14	
Decubitus ulcers (+)	9	4	.17
Catheterization (+)	23	18	.43
Nasogastric tube	17	12	.36
Tracheal tube	3	2	.72
Urethral tube	13	8	.28
WBC count, cells/mL*	9000 ± 3400	8600 ± 4500	.65
Hemoglobin, g/dL*	11.6 ± 1.8	11.1 ± 1.9	.28
CRP, mg/dL*	4.2 ± 4.8	4.8 ± 5.9	.63
Total protein, g/dL*	6.5 ± 0.7	6.8 ± 0.8	.14
AST, IU/L*	28 ± 17	24 ± 9.7	.20
ALT, IU/L*	23 ± 18	20 ± 17	.52
BUN, mg/dL*	22 ± 10	23 ± 13	.60
Cr, mg/dL*	0.9 ± 0.6	0.7 ± 0.4	.10

WBC, white blood cell; CRP, C-reactive protein; AST, aspartate aminotransferase; ALT, alanine aminotransferase; BUN, blood urea nitrogen; Cr, creatinine.
* Values are expressed as mean ± standard deviation.

Table 2. *Comparison of the Reduction and Disappearance Rates of Methicillin-Resistant* Staphylococcus aureus *in Sputum Between the Catechin Group and the Control Group*

	Numbers of Patients		
	Catechin Group	Control Group	*P* Value
Total patients (n = 69)	n = 36	n = 33	
Reduction†	17 (47%)	5 (15%)	.014*
Disappearance	11(31%)	4 (12%)	.091
Colonized patients (n = 53)	n = 26	n = 27	
Reduction	13 (50%)	5 (19%)	.027*
Disappearance	8 (31%)	4 (15%)	.40
Infected patients (n = 16)	n = 10	n = 6	
Reduction	4 (40%)	0 (0%)	.12
Disappearance	3 (30%)	0 (0%)	.89

* $P < .05$

† Reduction: the summation of decrease and disappearance of methicillin-resistant *Staphylococcus aureus*.

tion with imipenem, panipenem, or ceftazidime. No adverse events, such as respiratory tract obstruction, allergic bronchial spasm, or skin eruption, including laboratory changes, were observed in all patients during the study.

DISCUSSION

The present study demonstrating the effects of tea catechin inhalation on MRSA in a prospective randomized controlled manner is the first to be reported in the literature. The results showed that tea catechin inhalation for 1 week appeared to be effective in reducing the MRSA count when compared with saline inhalation alone. The results are consistent with those of our previous pilot study on the effects of a 4-week inhalation period of tea catechin on MRSA as compared to saline/bromhexine inhalation.[17] Furthermore, the tendency of reduction in MRSA counts was also observed in the colonized patients who were not administered any antibiotics. This tendency was also observed in the infected patients, however this was not significant probably due to the small sample size.

Despite a significant decrease in MRSA counts, the effect of tea catechin on MRSA was not sufficiently strong as to induce a complete eradication of MRSA from sputum. In our previous pilot study, we had observed that the effect of tea catechin inhalation on MRSA was greatest at 1 week of inhalation, however this effect was transient.[17] Therefore, the inhalation method has limited application as a supplementary treatment in combination with the standard therapy for the control of MRSA. Additionally, we should consider some of the limitations of the present study. First, the study design was not completely blinded. Although none of the patients participating in the study or their guardians were informed of the type of material used in the nebulizer, they could identify the material based on their knowledge of the color of tea catechin solution as transparent yellow and that of saline as colorless. Second, tea catechin is not an approved drug; therefore thorough informed consent is essential prior to participation in the study. Additionally, to ensure quality, the solution should be carefully prepared in a hospital clean room under sterile conditions.

The precise mechanism of action of tea catechin against MRSA has not yet been fully elucidated. Some natural products, such as vegetables and fruits, are reported to exhibit inhibitory effects on microorganisms.[20] Among them, tea catechins, a group of natural-occurring polyphenols, possess strong antioxidative activity, and the production of hydrogen peroxide is reported to be involved in the bactericidal activity against several bacterial strains, including MRSA.[21] Recent experimental studies have revealed that EGCG, the major low-molecular-weight polyphenol in green tea leaf extracts, is the main causative component of antibacterial activity and induces synergistic effects with antibiotics against MRSA.[7–15] EGCG can reverse methicillin resistance in MRSA in vitro. This phenomenon can be explained by the prevention of penicillin-binding protein 2' (PBP2') synthesis and inhibition of beta-lactamase secretion.[7] MIC of EGCG against MRSA was reported to be 100 μg/mL or less, and EGCG concentration less than the MIC value reversed the high level resistance of MRSA to beta-lactams.[9] Combinations of EGCG along with some non-beta-lactam antibiotics were also reported to show additive effects.[11,12] We also observed that tea catechins showed antimicrobial activity and induction of synergistic effects with some antibiotics, such as oxacillin, ceftazidime, imipenem, or vancomycin (data not shown in text). The result that tea catechins have the ability to restore the activity of antibiotics that have lost their potency against MRSA is of clinical importance since the overuse of antibiotics has led to development of antibiotic-resistant strains.

Natural chemical products, such as acetic acid and hypertonic saline as well as tea catechins, are known to possess antimicrobial activity.[22–24] With regard to a possible mechanism of inhalation effect of these agents on bacteria, it has been speculated that the hyperosmolarity of the nebulized solution may play an important role in the prevention of bacterial infections of the respiratory tract along with the improvement in mucociliary transport and removal from submucosal and adventitial edema.[23,24]

Precise information on recommended dosage, therapeutic window of tea catechin against MRSA, or concomitant drug interaction has not yet been obtained. In the pharmacokinetic study of tea catechin, low systemic bioavailability has been reported in the literature.[25] Therefore, inhalation might be suitable for reaching the site of action in the respiratory tract, and this therapy is speculated to cause less systemic adverse effects with effective dosage.

Tea catechins have been reported to be well tolerated, except in tea-factory workers with occupational asthma induced by the inhalation of green tea dust.[26,27] Moreover, the serum aspartate aminotransferase and creatinine levels are not altered following the consumption of tea catechin at concentrations up to 1000 mg/d for 3 months in normal volunteers.[28] The study also confirmed that no harmful side effects were observed in the elderly patients during 7 days of inhalation at a concentration of 22.2 mg/d using a handheld nebulizer. Although the results should be carefully interpreted because the sample size was small, catechin inhalation might be a safe supplementary treat-